Czech Technical University in Prague
Faculty of Electical Engineering
Department of Electromagnetic Field

Application of electron–light–wave analogy into metamaterials

Doctoral thesis

Mgr. Ivana Hrebíková

PhD programme: Electrical Engineering and Information Technology (P2612)
Branch of study: Radioelectronics (2601V010) Prague, January 2019

Supervisor: ass. Prof. Ing. Lukáš Jelínek, Ph.D
Co-supervisor: prof. Ing. Jan Macháč, DrSc.

Abstrakt

Dizertační práce se zabívá aplikací analogií mezi elektronovými a electromagnetickými vlnami a její následní aplikaci v návrhu polovodičových heterostruktur. V úvodní části je stručne zhrnut spůsob řešení nerelativistické bezčasové Schrödingerovy rovnice pomocí Kaneovy metody a tzv. *envelope function* formalismu. Pro úplnost je část doplněna o teoretický popis šíření electromagnetických vln. V hlavní části jsou představeny analogie mezi elektromagnetickými a elektronovými vlnami pro planárne a sférické struktury a jsou navrhuty dvě nové polovodičové heterostruktury. Prvním je návrh dokonalé čočky pro elektrony. Druhým návrhem je otevřený rezonátor, který podporuje vázané stavy v kontinuu.

Klíčové slova:

Metamateriály, analogie mezi světelnými a electronovými vlnami, Kane-ův model, formalizmus obálkové funkce, pseudopotenciál, dokonalá čočka pro elektrony, vázané kvantové jámy, otevřený rezonátor, core–shell rezonátor, vázané stavy v kontinuu

Abstract

The thesis focuses on analogies between electron waves and electromagnetic waves and their subsequent application into design of semiconductor heterostructures. The introductory part of the work briefly summarizes the Kane's method, envelope function formalism for evaluation of non–relativistic time–independent Schrödinger equation, and time–independent electromagnetic wave equation. The core part of the thesis presents analogies between electromagnetic– and electron–plane waves and spherical waves and proposes two novel designs. The first is a design of a perfect lens for electrons. The second design is an open core–shell resonator supporting bound states in continuum.

Keywords:

Metamaterials, electron–light–wave analogy, Kane's model, envelope function formalism, pseudopotential, perfect lens, bound quantum wells, open resonator, core–shell resonator, bound states in continuum.

Acknowledgements

First of all, I would like to express my gratitude to my dissertation thesis supervisor, ass. Prof. Ing. Lukáš Jelínek, Ph.D. He has been a constant source of encouragement and insight during my research and helped me with numerous problems and professional advancements. I would like to thank to prof. Ing. Jan Macháč, DrSc. for providing most of the funding for my research. Special thanks go to my colleagues from the Department of Electromagnetic Field, who maintained a pleasant and flexible environment for my research. Finally, my greatest thanks go to my family members, for their infinite patience and care and support.

Declaration of originality

I, the undersigned, hereby declare that this doctoral thesis is the result of my research in our research team. The thesis was written under the professional supervision of ass. Prof. Ing. Lukáš Jelínek, Ph.D using the literature and resources listed in the Bibliography and References.

In Prague, 15th January 2019, ...

Abbreviations

Physical Quantities, Symbols and Signs

$\hbar$	reduced Planck's constant
m_e	electron mass
m	dispersive mass of electron
ω	angular frequency
ε_0	dielectric constant of vacuum
ε_r	relative dielectric constant
μ_0	permeability of vacuum
μ_r	relative permeability
k_0	wavenumber in vacuum
f_c	wave–function of an electron
τ	life time
E	eigen energy of the electron
P	Kane's parameter
Γ_6	conduction electron band
Γ_7	split–off holes band
Γ_8	heavy and light holes band
E_{Γ_6}	band edge energy of the band Γ_6
E_{Γ_7}	band edge energy of the band Γ_7
E_{Γ_8}	band edge energy of the band Γ_8

E_c	conduction band energy
E_v	valence band energy
E_g	energy band gap
Δ	narrow band gap
T	transmission coefficient
R	radius
$\psi\left(\boldsymbol{r}\right)$	electron wave function
$V\left(\boldsymbol{r}\right)$	potential energy
$\boldsymbol{k} = \begin{pmatrix} k_x & k_y & k_z \end{pmatrix}$	wave vector
$\boldsymbol{E} = \begin{pmatrix} E_x & E_y & E_z \end{pmatrix}$	vector of the electric intensity
$\boldsymbol{H} = \begin{pmatrix} H_x & H_y & H_z \end{pmatrix}$	vector of the magnetic intensity

Mathematical Operators

∇	nabla operator
$\frac{\partial}{\partial x}, \frac{\partial}{\partial y}, \frac{\partial}{\partial z}$	partial derivatives
$\hat{\mathrm{H}}$	Hamilton operator

Miscellaneous Abbreviations

BIC	Bound states in continuum
ENZ	Epsilon near zero
FCC	Face–centered cubic
HgTe	Mercury Telluride
HgCdTe	Mercury Cadmium Telluride
LPM	Local pseudopotential method
OPW	Orthogonal plane wave
TE wave	Transverse electric wave
TM wave	Transverse magnetic wave

List of Figures

List of Tables

Contents

Introduction

An analogy is a basic principle of understanding nature, where it joints different phenomena linked by common properties or similar behavior. Such occurrence can be found in many areas, not only in physics. A well known example is medicine, where developed treatment is firstly tested on animals with a similar reaction to human. Another example is biology where scientists use the knowledge of current fauna to research into extinct species on the bases of species similarities, e.g. how they moved, what they eat, etc. This work focuses on analogies between different areas of physics, namely classical electromagnetism and non–relativistic quantum mechanics.

Although the existence of quantum–classical analogy is well–known since the early years of quantum mechanics, its experimental verification has become relevant only in recent years, since technological achievements have made possible to prepare quantum systems with classical–type behavior or classical systems with quantum–type behavior. For example, technologies allowing semiconductor structures, in which electrons can propagate without interactions with other electrons or ions, support the description of ballistic electrons under the effective–mass approximation and thus as quantum–mechanical waves, which can reflect, refract, diffract and scatter during propagation, and can even interfere in the same manner as electromagnetic waves. This feature is quite surprising due to the difference between the electrons and photons in almost every aspect, such as rest mass (finite for electrons, zero for photons), spin (1/2 spin for electrons, 1 for photons), charge (negative for electrons, no charge for photons), dispersion (parabolic for electrons, linear for photons) and quantum statistics (Fermi-Dirac for electrons and Bose-Einstein for photons). There are two possibilities of employing the electron–electromagnetic–waves analogy — what the quantum mechanics can teach us and is simultaneously applicable into electromagnetism, and vice versa. An example of the first possibility, i.e. what quantum mechanics has brought into electromagnetism, is an idea of a photonic band gap that has brought important new concept how to control the light propagation through media.

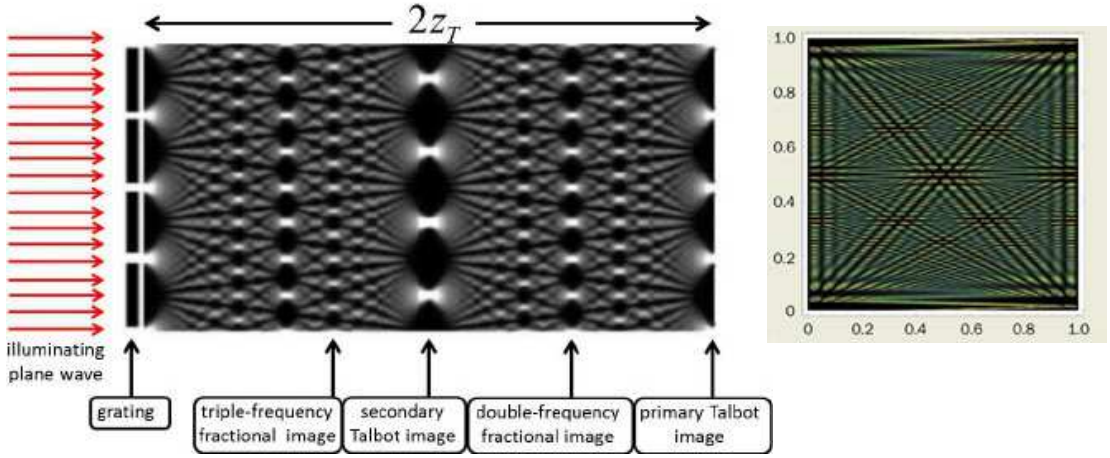

Figure 1: (left) An example of Talbot effect, or near–field diffraction effect. The figure shows an image of a grating in repetition at regular distances away from the grating plane [1]. Similarly, so–called quantum carpets [2] represent quantum wave packet as electron in an atom (right).

The concept is based on knowledge of propagation of an electron in a crystalline lattice — periodically positioned atoms — which shows that there are only certain energies allowing electron propagation and which are represented by a bandstructure. Further development of photonic band gap structures opened a new part of the electromagnetic theory known as photonic crystals [3], which have had major impact on the design of optical fibers [4, 5, 6], mirrors [7, 8], filter transmission [9], and waveguide splitters [10, 11].

A design of electromagnetic periodic structures and arrays has brought also other effects, not only photonic band gaps, that had not been observed in the existing solutions. Many of these effects had been explained in quantum mechanics and thus their quantum description was facilitated in electromagnetism. An illustrative example is a periodic motion of wave packets in a homogeneous electric field firstly observed in 2004 [12], nowadays known as optical Bloch oscillations. A similar phenomenon occurs also in crystalline lattices when a DC electric field is applied. Caused periodical motions of electrons (Bloch oscillations) driven by this electric field were pointed out by Bloch [13] and Zener [14] early in the previous century and later also experimentally confirmed [15].

The analogy between quantum mechanics and electromagnetism has also initiated the collaboration between these two fields. One of the interesting phenomena in quantum mechanics is the bound state in continuum (BIC). The BICs were predicted for specific potentials by von Neumann and Wigner in 1929 [16]. Their work was later extended to a

two–electron wave function [17], still wearing the sign of BIC. More recently it has been proposed that the BICs can be decoupled from all continuum states also by virtue of symmetry [18, 19, 20]. Experimental observation of BICs has not yet been achieved [21].

Resonant states in the continuum have recently elicited significant interest in the field of photonics. Indeed, for light waves it may be easier to design a resonator environment at will using photonic crystals or metamaterials [22, 23, 24, 25, 26]. Photonic crystals even made an experimental observation of BICs possible [27, 28, 29]. In this context, BICs may be regarded as limiting cases of leaky waves. The usual leaky–wave states discussed in the electromagnetism literature are excitations with a finite lifetime and are in some sense the analog of electronic "resonant states". Thus, a BIC may be seen as the limit of a leaky state with vanishingly small resonance width [28, 29, 30].

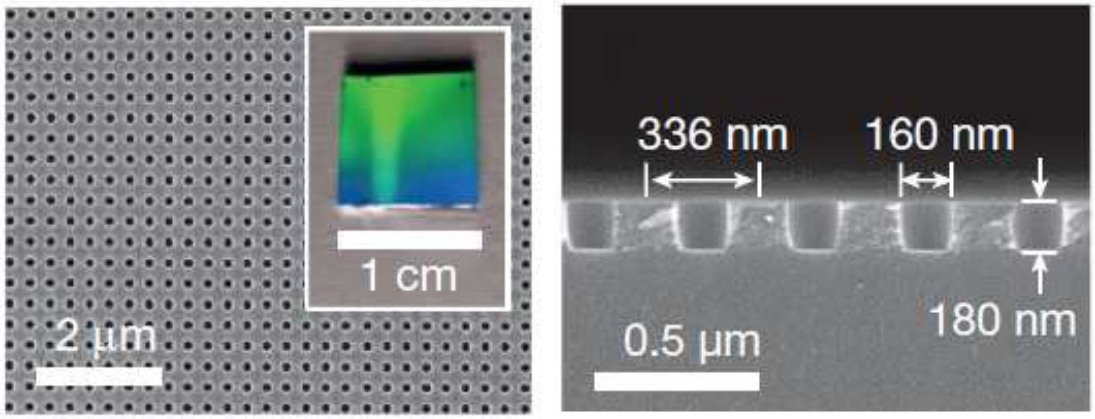

Figure 2: SEM images of the photonic structure supporting optical bound states within the continuum – top (left) and side (right) view [31].

It cannot be left unnoticed that there are also other photonic structures inspired by quantum mechanics such as quantum wells [32], quantum wires [33] or quantum dots [34].

The second point of view on the analogy between electron– and light–waves is "What can electromagnetism bring into quantum mechanics?" Due to the wave description of electron motion in semiconductors and thus its ability to reflect, refract, diffract and interfere, similarly as light waves, and due to the possibility of the precise monolayer growth of semiconductors, the quantum–classical analogy has contributed significantly also in the development of semiconductor environment. Many semiconductor devices based on this analogy have been proposed and also experimentally demonstrated. As representative examples can be mentioned electrostatic or magnetic lenses [35, 36, 37], prism [38], electron

beam splitter [39], directional couplers [40, 41], filters [42], circuit theory concepts [43]. Unfortunately, developments in this field peaked well before the emergence of metama-

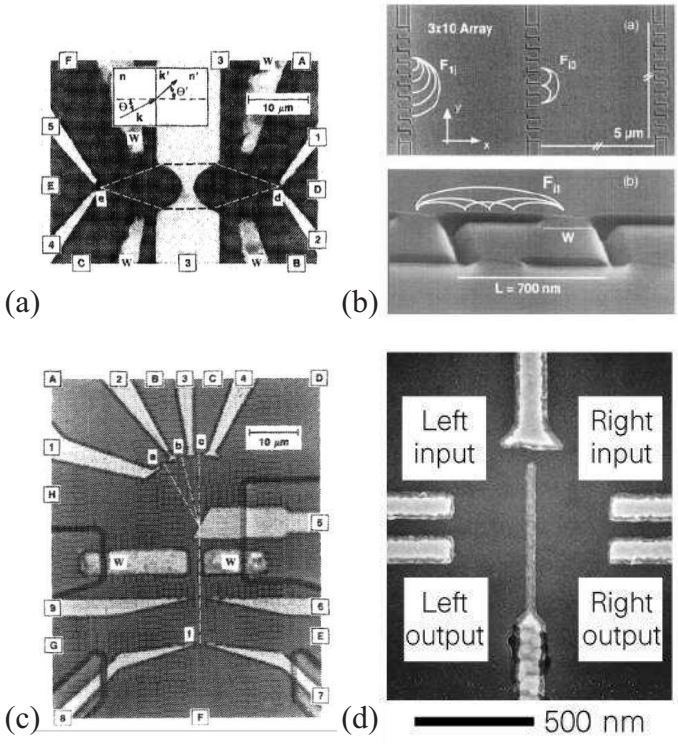

Figure 3: Examples of semiconductor devices which have been inspired by their electromagnetic counterparts. a) Electrostatic lens [35], b) magnetic lens [36], c) electron prism [38], d) electron beam splitter [39]

terials, i.e., composite materials offering electromagnetic properties not found in natural substances, such as negative permittivity and permeability [44, 45]. Metamaterials have brought important new concepts into classical electromagnetism, e.g. the perfect lens [46] and transformation optics [47, 48], while their quantum analogies have not received the attention that they deserve, with the exception of a few pioneering studies that will be briefly reviewed. In [49], a particularly simple form of the analogy of an electromagnetic plane wave and an electron wave is presented. The author then transfers the idea of complementary media into the electron domain using transmission matrix formalism, and proposes using the complementary medium layer to improve the scanning tunneling microscopy of specific structures. Paper [50] uses the analogy presented in [49] to explore the I–V characteristics and the traversal times of ballistic electrons propagating normally to the boundaries of the heterostructure analogous to the metamaterial perfect lens. The

electron analogy of a perfect lens was further proposed in the form of a p-–n junction on a graphene sheet [51]. In [52] it was shown that spatial transformations leading to transformation optics and to metamaterial cloaking can also be used in a very similar manner used on the Schrödinger equation. Later, in [53], it was shown that ballistic electrons propagating in the HgTe-–CdTe heterostructure can exhibit perfect tunneling, a phenomenon largely responsible for the unique properties of the perfect lens. Important papers [54, 55] then showed that envelope approximation, commonly used for describing ballistic electrons in semiconductor heterostructures, is equivalent to the effective medium theory commonly used for describing of electromagnetic metamaterials. By means of this effective medium, a perfect lens made of graphene [55] was proposed. Lastly, the analogies mentioned above were used for a study of the cloaking of matter waves [56, 57, 58].

Goal of Thesis

This doctoral thesis is focused on applications of the analogy between quantum–mechanics and electromagnetic wave. Based on the analogy,

- a perfect lens for electrons (Chap. 3);
- an open perfect resonator for electrons (Chap. 4)

is proposed. In order to achieve these key objectives, several steps need to be taken, namely:

- approval of the analogy between electron– and electromagnetic–wave (planar system Sec. 3.1, spherical system Sec. 4.1);
- study the design in electromagnetic case and propose its quantum–mechanical counterpart (perfect lens - Sec. 3.2, open resonator – Sec. 4.2);
- discuss the proposed design (perfect lens – Secs. 3.2, and 3.3, open resonator – Secs. 4.3, 4.4, and 4.5).

Chapter 1

Electron as an Envelope Function

The similar behavior of an electron– and light–wave has been proved by experiments as well as by theory. In the current state of the art, there are several models of this analogy and it is therefore essential to show on which this thesis is built on.

Understanding of electron propagation in solids is connected with a solution to Schrödinger equation for the whole system of electrons and atomic cores including their interactions. However, providing that only valence–electron propagation is considered and noting that the mass of the ion core (core electrons with the nucleus) is much greater than the mass of the valence electron, it is a common practice [59] to assume that every valence electron interacts only with a given background potential $V(\boldsymbol{r})$. Within this mean–field approximation [59], the problem of an electron propagation via a solid is described by one electron time–independent Schrödinger equation [60]

$$\hat{\mathrm{H}}_{1\mathrm{e}}\psi_n(\boldsymbol{r}) = E_n\psi_n(\boldsymbol{r}), \tag{1.1}$$

where $\hat{\mathrm{H}}_{1\mathrm{e}}$ is one–electron Hamiltonian, $\psi_n(\boldsymbol{r})$ and E_n are, respectively, the wave function and energy of the electron in an n-th eigenstate.

The one–electron Hamiltonian

$$\hat{\mathrm{H}}_{1\mathrm{e}} = \frac{-\hbar^2}{2m_{\mathrm{e}}}\nabla^2 + V_{\mathrm{eff}}(\boldsymbol{r}) \tag{1.2}$$

expresses an energy of the whole system. Provided that effective potential $V_{\mathrm{eff}}(\boldsymbol{r})$ is known, Schrödinger equation (1.1) is a linear three–dimensional eigenvalue problem, where the spectrum of energies E_n represents the eigenstates of an electron in the effective potential. Many useful transport properties can be derived from the spectrum of allowed energies itself. It is worth mentioning that the equation is not assuming spin of electron. The term

describing spin interactions (for example spin orbit coupling) does not significantly affect theoretical prediction described in this thesis and is therefore, intentionaly, ommited.

There are several standard methods of bandstructure computation for semiconductors, and all of them involve approximations which emphasize some aspects of the electronic properties of semiconductors while, at the same time, de–emphasizing other aspects. In general, the methods can be divided into two groups depending on the way of determining the potential $V_{\text{eff}}(\boldsymbol{r})$. The first group contains methods which calculate bandstructures from first principles; without a need of any empirical parameters. These methods are called *ab initio* methods and commonly utilize variational approach to calculate a ground state energy of a many–body system, where the system is defined at the atomic level. To this category belong methods such as Hartree–Fock or Density Functional Theory [61]. The second group contains empirical methods such as tight–binding method [62, 63], the local or non–local empirical pseudopotential method [64], and the $\boldsymbol{k}\cdot\boldsymbol{p}$ envelope function method [65, 66]. These methods utilize empirical parameters usually obtained from experimental data or above mentioned *ab initio* methods. The advantage of these empirical methods is that the electronic bandstructure can be calculated from the one–electron time–independent Schrödinger equation. In this thesis we will mostly employ the $\boldsymbol{k}\cdot\boldsymbol{p}$ envelope function method and for specific purposes (see Sec.3.2) of verification we will also use local pseudopotential method (Appendix A).

1.1 $\boldsymbol{k}\cdot\boldsymbol{p}$ Method

The $\boldsymbol{k}\cdot\boldsymbol{p}$ method was developed for exploring the properties of the energy bands and wave functions in the vicinity of some important points in the $\boldsymbol{k}$–space with the aid of a perturbation theory. The advantage of $\boldsymbol{k}\cdot\boldsymbol{p}$ method is that the bandstructure in the vicinity of a point in $\boldsymbol{k}$–space can be reached using just a small number of parameters which may be determined experimentally. Treating the one–electron problem of an electron propagation in a periodic potential $V(\boldsymbol{r})$

$$\hat{\mathrm{H}}_{1\mathrm{e}}\psi(\boldsymbol{r}) = \left[-\frac{\hbar^2}{2m_{\mathrm{e}}}\nabla^2 + V(\boldsymbol{r})\right]\psi(\boldsymbol{r}) = E\psi(\boldsymbol{r}) \tag{1.3}$$

Bloch showed that $\psi(\boldsymbol{r})$ may be written as

$$\psi(\boldsymbol{r}) = \mathrm{e}^{\mathrm{i}\boldsymbol{k}\cdot\boldsymbol{r}}u_{n\boldsymbol{k}}(\boldsymbol{r}), \tag{1.4}$$

where $u_{n\boldsymbol{k}}(\boldsymbol{r})$ has the periodicity of $V(\boldsymbol{r})$ and forms a complete set of cell periodic functions for any $\boldsymbol{k}$ lying in the first Brillouin zone [60]. The index n designates a band and runs over a complete set of bands. From this it follows that if the energy and momentum matrix elements are known for all bands for any given value of $\boldsymbol{k}$, the energies for all $\boldsymbol{k}$ are completely determined.

Substituting Eq. (1.4) into (1.3) gives

$$\left[\frac{p^2}{2m_\mathrm{e}} + \frac{\hbar}{m_\mathrm{e}}\boldsymbol{k}\cdot\boldsymbol{p} + \frac{\hbar^2 k^2}{2m_\mathrm{e}} + V(\boldsymbol{r})\right] u_{n\boldsymbol{k}}(\boldsymbol{r}) = E_n(\boldsymbol{k})\, u_{n\boldsymbol{k}}(\boldsymbol{r}), \tag{1.5}$$

whereby momentum $\boldsymbol{p} = -\mathrm{i}\hbar\nabla$ was introduced. As was mentioned above, for any given $\boldsymbol{k}$, the set of $u_{n\boldsymbol{k}}(\boldsymbol{r})$ is complete for functions having the same periodicity as the potential $V(\boldsymbol{r})$. Hence, choosing $\boldsymbol{k} = \boldsymbol{k}_0$, the wave function for any $\boldsymbol{k'}$ in the vicinity of $\boldsymbol{k}_0$ may be expressed as follows

$$u_{n\boldsymbol{k'}}(\boldsymbol{r}) = \sum_{n'} c_{n'n}(\boldsymbol{k'} - \boldsymbol{k}_0)\, u_{n'\boldsymbol{k}_0}(\boldsymbol{r}). \tag{1.6}$$

In other words, once the solution of the one–electron problem

$$\hat{\mathrm{H}}_{\boldsymbol{k}_0} u_{n\boldsymbol{k}_0} = E_n(\boldsymbol{k}_0)\, u_n\boldsymbol{k}_0 \tag{1.7}$$

is known, the solution for any $\boldsymbol{k}$ in the vicinity of $\boldsymbol{k}_0$ is given by the following equation

$$\left(\hat{\mathrm{H}}_{\boldsymbol{k}_0} + \frac{\hbar}{m_\mathrm{e}}(\boldsymbol{k} - \boldsymbol{k}_0)\cdot\boldsymbol{p} + \frac{\hbar^2}{2m_\mathrm{e}}\left(k^2 - k_0^2\right)\right) u_{n\boldsymbol{k}} = E_n(\boldsymbol{k})\, u_{n\boldsymbol{k}}, \tag{1.8}$$

where

$$\hat{\mathrm{H}}_{\boldsymbol{k}_0} = \frac{p^2}{2m_\mathrm{e}} + \frac{\hbar^2}{m_\mathrm{e}}\boldsymbol{k}_0\cdot\boldsymbol{p} + \frac{\hbar^2 k_0^2}{2m_\mathrm{e}} + V(\boldsymbol{r}). \tag{1.9}$$

Equation (1.8) can easily be converted into a matrix eigenvalue equation by substituting Eq. (1.6) into (1.8), multiplying both sides of Eq. (1.8) by $u_{n\boldsymbol{k}_0}$, and integrating over the unit cell. Thence equation (1.8) enters the form

$$\sum_{n'}\left[\left\{E_n(\boldsymbol{k}_0) + \frac{\hbar^2}{2m_\mathrm{e}}\left(k^2 - k_0^2\right)\right\}\delta_{nn'} + \frac{\hbar}{m_\mathrm{e}}(\boldsymbol{k} - \boldsymbol{k}_0)\cdot\boldsymbol{p}_{nn'}\right] c_{n'n} = E_n(\boldsymbol{k})\, c_{n'n}, \tag{1.10}$$

where

$$\boldsymbol{p}_{nn'} = \int_{\text{unit cell}} u^*_{n\boldsymbol{k}_0}(r)\, \boldsymbol{p} u_{n'\boldsymbol{k}_0}(r)\, \mathrm{d}\boldsymbol{r}. \tag{1.11}$$

If we look at the third term of the sum one can notice that $\hbar/m_\mathrm{e}(\boldsymbol{k} - \boldsymbol{k}_0)\cdot\boldsymbol{p}_{nn'}$ are off–diagonal and when $\boldsymbol{k}$ is close to $\boldsymbol{k}_0$, the term can be treated as a perturbation. Corresponding eigenvalues and eigenvectors can be calculated using the perturbation theory [67].

In semiconductors, the bands of interest are primarily valence band and the conduction band. In such a case, it is common to introduce a new indexing $n = \mathrm{c}$ and $n' = \mathrm{v}$ for conduction band and valence band, respectively. Focusing on these states, (1.10) can be written as

$$\begin{vmatrix} E_c(\boldsymbol{k}_0) - E_c(\boldsymbol{k}) + \dfrac{\hbar^2}{2m_\mathrm{e}}(k^2 - k_0^2) & \dfrac{\hbar}{m_\mathrm{e}}(\boldsymbol{k} - \boldsymbol{k}_0)\cdot\boldsymbol{p}_{cv} \\ \dfrac{\hbar}{m_\mathrm{e}}(\boldsymbol{k} - \boldsymbol{k}_0)\cdot\boldsymbol{p}_{cv} & E_v(\boldsymbol{k}_0) - E_v(\boldsymbol{k}) + \dfrac{\hbar^2}{2m_\mathrm{e}}(k^2 - k_0^2) \end{vmatrix} = 0 \qquad (1.12)$$

which eigenvalues are

$$E(\boldsymbol{k}) = \frac{1}{2}\left[E_c(\boldsymbol{k}_0) + E_v(\boldsymbol{k}_0) + \frac{\hbar^2}{m_\mathrm{e}}\left(k^2 - k_0^2\right)\right] \pm \\ \pm \frac{1}{2}\left[\left(E_c(\boldsymbol{k}_0) - E_v(\boldsymbol{k}_0)\right)^2 + \frac{4\hbar^2}{m_\mathrm{e}^2}|(\boldsymbol{k} - \boldsymbol{k}_0)\cdot\boldsymbol{p}_{cv}|^2\right]^{\frac{1}{2}}. \qquad (1.13)$$

For most applications, only the top/bottom of valence/conduction band is of interest. Therefore, the point of evaluation $\boldsymbol{k_0}$ is placed at the Γ point, i.e., $\mathrm{k}_0 = 0$. Then the solution (1.13) for small $\boldsymbol{k}\cdot\boldsymbol{p}_{\mathrm{cv}}$ is given by

$$E(\boldsymbol{k}) = \begin{cases} E_\mathrm{c} - E_\mathrm{v} + \dfrac{\hbar^2 k^2}{2m_\mathrm{e}} + \dfrac{\hbar^2}{(E_\mathrm{c} - E_\mathrm{v})\, m_\mathrm{e}^2}|\boldsymbol{k}\cdot\boldsymbol{p}_{\mathrm{cv}}|^2 & \text{conduction band} \\ \dfrac{\hbar^2 k^2}{2m_\mathrm{e}} - \dfrac{\hbar^2}{(E_\mathrm{c} - E_\mathrm{v})\, m_\mathrm{e}^2}|\boldsymbol{k}\cdot\boldsymbol{p}_{\mathrm{cv}}|^2 & \text{valence band} \end{cases} \qquad (1.14)$$

where the term $E_\mathrm{c} - E_\mathrm{v}$ is commonly known as energy band gap E_g.

For simple representation of semiconductor bandstructure this 2–band model is sufficient. Nevertheless, for a more precise description of semiconductors it is necessary to consider the degeneration of the valence band and also inter–band interactions.

The conduction bands (Γ_6 group) originate primarily from the outermost atomic cation s–states, whereas the top of valence bands consisting of heavy hole band, light hole band (Γ_8 group) and split–off band (Γ_7 group) result from the outermost atomic anion p–states . Since the conduction band at $\boldsymbol{k} = 0$ is invariant under the space symmetry operations, one denotes these functions by $|S\rangle$. On the other hand, the uppermost 3 valence band states at Γ transform like $|X\rangle$, $|Y\rangle$, $|Z\rangle$. However, these three functions do not form a basis of an irreducible representation of the Hamiltonian. The solution of the problem can be found in a linear combination of these states. One can show [68] that the following linear combination of $\boldsymbol{k} = 0$ Bloch states yields the band edge values as shown in Table 1.1.

Table 1.1: Definition of new Bloch basis defined as a linear combination of the $|S\rangle$, $|X\rangle$, $|Y\rangle$, $|Z\rangle$.

State	Combination	Energy at Γ	Group
$\|u_1\rangle$	$\mathrm{i}\,\|S\rangle$	E_g	Γ_6
$\|u_2\rangle$	$\sqrt{\frac{1}{2}}\left(\|X\rangle - \mathrm{i}\,\|Y\rangle\right)$	0	Γ_8
$\|u_3\rangle$	$-\sqrt{\frac{2}{3}}\,\|Z\rangle - \sqrt{\frac{1}{6}}\left(\|X\rangle - \mathrm{i}\,\|Y\rangle\right)$	0	Γ_8
$\|u_4\rangle$	$\sqrt{\frac{1}{3}}\,\|Z\rangle - \sqrt{\frac{1}{3}}\left(\|X\rangle - \mathrm{i}\,\|Y\rangle\right)$	$-\Delta$	Γ_7

Once the Bloch states at $\boldsymbol{k_0} = 0$ and corresponding energies are known, i.e., solution of equations

$$\begin{aligned}
\hat{\mathrm{H}}_0 u_{1,0} &= E_{\mathrm{c},0} u_{1,0} \\
\hat{\mathrm{H}}_0 u_{2,0} &= E_{\mathrm{v},0} u_{2,0} \\
\hat{\mathrm{H}}_0 u_{3,0} &= E_{\mathrm{v},0} u_{3,0} \\
\hat{\mathrm{H}}_0 u_{4,0} &= E_{\mathrm{v},0} u_{4,0}
\end{aligned} \tag{1.15}$$

is known, the Hamiltonian $\hat{H}_{4\mathrm{x}4}$ for non–zero $\boldsymbol{k}$ can be written. The individual terms of the matrix are shown in Table 1.2.

Table 1.2: Elements of the Hamiltonian matrix.

	$\|u_1\rangle$	$\|u_2\rangle$	$\|u_3\rangle$	$\|u_4\rangle$
$\|u_1\rangle$	$E_g + \frac{\hbar^2 k^2}{2m_\mathrm{e}}$	$-\sqrt{\frac{2}{3}}\frac{P\hbar k_z}{m_\mathrm{e}}$	$\frac{P\hbar k_+}{m_\mathrm{e}}$	$\sqrt{\frac{1}{3}}\frac{P\hbar k_z}{m_\mathrm{e}}$
$\|u_2\rangle$	$-\sqrt{\frac{2}{3}}\frac{P\hbar k_z}{m_\mathrm{e}}$	$\frac{\hbar^2 k^2}{2m_\mathrm{e}}$	0	0
$\|u_3\rangle$	$\frac{P\hbar k_-}{m_\mathrm{e}}$	0	$\frac{\hbar^2 k^2}{2m_\mathrm{e}}$	0
$\|u_4\rangle$	$\sqrt{\frac{1}{3}}\frac{P\hbar k_z}{m_\mathrm{e}}$	0	0	$-\Delta + \frac{\hbar^2 k^2}{2m_\mathrm{e}}$

where nomenclatures $k_\pm = \frac{1}{\sqrt{2}}\left(k_x \pm \mathrm{i}k_y\right)$, energy band gap $E_\mathrm{g} = E_{\Gamma_6} - E_{\Gamma_8}$ and narrow gap $\Delta = E_{\Gamma_8} - E_{\Gamma_7}$ were introduced. The Kane's parameter P defined as

$$P = -\mathrm{i}\,\langle S\,|p_x|\,X\rangle = -\mathrm{i}\,\langle S\,|p_y|\,Y\rangle = -\mathrm{i}\,\langle S\,|p_z|\,Z\rangle \tag{1.16}$$

represents conduction–valence band interactions.

Finding eigenvalues $E(\boldsymbol{k})$ is connected with solving the determinantal equation of the 4 by 4 $\boldsymbol{k}\cdot\boldsymbol{p}$ matrix given by the Table 1.2;

$$\varepsilon\left(\left(\varepsilon - E_{\mathrm{g}}\right)\varepsilon\left(\varepsilon+\Delta\right) - \frac{P^2\hbar^2k^2}{m_{\mathrm{e}}^2}\left(\varepsilon+\frac{2}{3}\Delta\right)\right) = 0. \tag{1.17}$$

Here, for the ease of presentation, the substitution $\varepsilon = E(\boldsymbol{k}) - \dfrac{\hbar^2k^2}{2m_{\mathrm{e}}}$ is used.

Introducing an effective mass, the solution of (1.17) can be written in reduced form

$$E_{n\boldsymbol{k}} = E_{n0} + \frac{\hbar^2k^2}{2m_n}, \tag{1.18}$$

where n denotes the band and E_{n0} means the band edge energy of corresponding band. For conduction band (Γ_6) the band edge effective mass is defined as

$$\frac{1}{m_{\Gamma_6}} = \frac{1}{m_{\mathrm{e}}} + \frac{2P^2}{3}\left(\frac{2}{E_{\mathrm{g}}} + \frac{1}{E_{\mathrm{g}}+\Delta}\right). \tag{1.19}$$

Up to this point, only isotropic, parabolic dispersion relation was assumed. Considering non–parabolic bands, an energy–dependent effective mass shall be defined via group velocity

$$v_{\mathrm{g}} = \frac{1}{\hbar}\frac{\partial E}{\partial k} = \frac{\hbar k}{m(E)}. \tag{1.20}$$

In such a case the effective mass is given

$$\frac{1}{m(E)} = \frac{1}{m_{\mathrm{e}}} + \frac{2P^2}{3}\left(\frac{2}{E+E_{\mathrm{g}}-E_{\Gamma_6}} + \frac{1}{E+E_{\mathrm{g}}-E_{\Gamma_6}+\Delta}\right). \tag{1.21}$$

Once the effective mass and the band edge energies are known, the bandstructure of a semiconductor is defined and hence the behavior of an electron in such the semiconductor can be predicted.

Aforementioned theory can be used not only to predict the bandstructure of a semiconductor and/or to depict some properties, but in special cases can be used as a tool for describing an electron propagation through a semiconductor heterostructure. However there has been developed a method for such application using an envelope function formalism. As is shown further, also this approach gives similar results.

1.2 Envelope Function Formalism

In realistic heterostructures, where each layer is composed of many atoms and wave vectors of the electron are small $k \ll 2\pi/a$, an alternative description of the valence electrons is possible. In such a case, it is possible to homogenize the microscopic wave function $\psi(\boldsymbol{r})$ and the potential $V(\boldsymbol{r})$ [65, 69, 54], resulting in an effective "macroscopic" wave function $\psi_{\text{eff}}(\boldsymbol{r}) = \langle\psi\rangle$, which varies slowly on the scale of the lattice constant, and in an effective potential $V_{\text{eff}}(\boldsymbol{r}) = \langle V\rangle$, which is a constant for each heterostructure layer [65, 69, 54, 70, 57, 55]. The brackets $\langle\,\rangle$ represent the operation of spatial averaging. This *envelopefunction* formalism was originally introduced by G. Bastard [69, 68, 71], and it was further reworked in recent studies [54, 57, 55]. The point of view of this article is based on the ideas of Ref. [54, 55].

An important observation is that $\psi_{\text{eff}} = \langle\psi\rangle$ does not imply that $|\psi_{\text{eff}}(\boldsymbol{r})|^2 = \langle|\psi|^2\rangle$, and hence $|\psi_{\text{eff}}(\boldsymbol{r})|^2$ does not generally represent the probability density. The spatially averaged probability density of energy eigenstates can be written in terms of ψ_{eff} as [54, 70, 72] (see Appendix B)

$$\langle|\psi|^2\rangle = \left(1 - \frac{\partial V_{\text{eff}}}{\partial E}\right)|\psi_{\text{eff}}|^2 + \frac{\hbar^2}{m^2}\frac{\partial m}{\partial E}\|\nabla\psi_{\text{eff}}\|^2. \tag{1.22}$$

Within this paradigm, the wave function ψ_{eff} satisfies the macroscopic time–independent Schrödinger equation

$$-\frac{\hbar^2}{2m}\Delta\psi_{\text{eff}}(\boldsymbol{r}) + V_{\text{eff}}\psi_{\text{eff}}(\boldsymbol{r}) = E\psi_{\text{eff}}(\boldsymbol{r}), \tag{1.23}$$

where $V_{\text{eff}} = E_{\Gamma_6}$ is the band edge energy of the conduction (Γ_6) band, and where m is dispersive mass [65, 69, 54, 55], defined as

$$\frac{1}{m} = \frac{1}{m_{\text{e}}} + \frac{2P^2}{3\hbar^2}\left(\frac{2}{E - E_{\Gamma_8}} + \frac{1}{E - E_{\Gamma_7}}\right). \tag{1.24}$$

This description is thus fully equivalent to the Kane's model presented in Sec. 1.1.

Chapter 2

Light as an Electromagnetic Wave

The aim of this work is to design metamaterial–like semiconductor structures. Since metamaterials originally belong to classical electrodynamics, equations describing the propagation of electromagnetic waves in a medium are briefly discussed in this chapter.

Mathematically, electromagnetic wave propagation differ from electron waves propagation in two major aspects:

- folds an electric and magnetic wave;
- has vector character.

Electromagnetic wave description, therefore, involves vector calculus, embodied in Maxwell's equations

$$\begin{aligned} \nabla \cdot \boldsymbol{D}(\boldsymbol{r},t) &= \rho_{\text{free}}(\boldsymbol{r},t) \\ \nabla \cdot \boldsymbol{B}(\boldsymbol{r},t) &= 0 \\ \nabla \times \boldsymbol{E}(\boldsymbol{r},t) &= -\frac{\partial \boldsymbol{B}(\boldsymbol{r},t)}{\partial t} \\ \nabla \times \boldsymbol{H}(\boldsymbol{r},t) &= \boldsymbol{J}_{\text{free}}(\boldsymbol{r},t) + \frac{\partial \boldsymbol{D}(\boldsymbol{r},t)}{\partial t} \end{aligned} \tag{2.1}$$

where

$\boldsymbol{E}$ – electric intensity

$\boldsymbol{H}$ – magnetic intensity

$\boldsymbol{D} = \varepsilon_0 \boldsymbol{E} + \boldsymbol{P}$ – electric flux density

$\boldsymbol{B} = \mu_0 (\boldsymbol{H} + \boldsymbol{M})$ – magnetic induction

$\boldsymbol{P}$ – electric polarization vector

$\boldsymbol{M}$ – magnetic polarization vector

$\boldsymbol{J}$ – current density

ρ_{free} – charge density of free charges

As presented, Maxwell's equations are macroscopic involving space and time averages of microscopic quantities [73, 74]. The reason for this approximation is the enormous complexity of microscopic charge and current densities inside a polarized matter, which will make the microscopic description intractable. Such description is thus equivalent to the use of effective atomic potential $V_{\text{eff}}(\boldsymbol{r})$ employed in Sec.1.1.

2.1 Propagation of electromagnetic waves

Propagation of electromagnetic waves in linear isotropic medium is best described in time–harmonic domain [75], i.e., under assumption

$$\begin{aligned} \boldsymbol{E} &= \tilde{\boldsymbol{E}}(\boldsymbol{r})\, e^{\mathrm{i}\omega t}, \\ \boldsymbol{H} &= \tilde{\boldsymbol{H}}(\boldsymbol{r})\, e^{\mathrm{i}\omega t}, \end{aligned} \tag{2.2}$$

where $\tilde{\boldsymbol{F}}$ is a phasor of the respective field, ω is an angular frequency and i denotes imaginary unit. Under this assumption, Maxwell's equations in source free region read

$$\begin{aligned} \nabla \cdot \tilde{\boldsymbol{E}} &= 0 \\ \nabla \cdot \tilde{\boldsymbol{H}} &= 0 \\ \nabla \times \tilde{\boldsymbol{E}} &= -\mathrm{i}\omega\mu\tilde{\boldsymbol{H}} \\ \nabla \times \tilde{\boldsymbol{H}} &= \mathrm{i}\omega\varepsilon\tilde{\boldsymbol{E}} \end{aligned} \tag{2.3}$$

which are also equivalent to a Helmholtz equation for an electric field

$$\Delta\tilde{\boldsymbol{E}} + k^2\tilde{\boldsymbol{E}} = 0 \tag{2.4}$$

or a magnetic field

$$\Delta\tilde{\boldsymbol{H}} + k^2\tilde{\boldsymbol{H}} = 0, \tag{2.5}$$

with k being a wave number, i.e.,

$$k = \omega\sqrt{\mu\varepsilon}. \tag{2.6}$$

Behavior of electromagnetic fields at medium interfaces is described by following boundary conditions

$$\begin{aligned} \boldsymbol{n} \times (\boldsymbol{E_2} - \boldsymbol{E_1}) &= 0 \\ \boldsymbol{n} \times (\boldsymbol{H_2} - \boldsymbol{H_1}) &= 0 \\ (\boldsymbol{D_2} - \boldsymbol{D_1}) \cdot \boldsymbol{n} &= 0 \\ (\boldsymbol{B_2} - \boldsymbol{B_1}) \cdot \boldsymbol{n} &= 0 \end{aligned} \tag{2.7}$$

where $\boldsymbol{n}$ is a unit normal to the corresponding medium interface. Equations (2.7) together with (2.4) and (2.5) guarantee unique field solution.

Comparison of Helmholtz equation (2.4) or (2.5) with time–independent Schrödinger equation (1.1) reveal apparent similarity that provides high probability of very similar propagative behavior of electron and light wave in a medium. Particularly, if ψ_n represents an electron wave and $\tilde{\boldsymbol{F}}$ represents, for instance, electric wave, then Hamiltonian $\hat{H}_{1\mathrm{e}}$ is quantum representative of ∇ operator and eigenenergy of electron E_n is classified in the same manner as the wave number k.

Chapter 3

Perfect Lens for Electron

One of the milestones in the matematerial research was the work in a perfect lens for electromagnetic waves [46]. Pendry in his paper showed that electromagnetic wave can propagate in an appropriate heterostructure from a source plane to an image plane with transmission coefficient equal to 1 [46]. In order to mimic this behavior in the case of electron waves, analogy between plane electromagnetic waves and ballistic electrons need to be studied.

3.1 Analogy between electron waves and light waves for planar systems

The topology of a perfect lens [46] is represented by a layered isotropic medium (stacking along the z-axis is assumed) in which oblique plane waves with the wave–vector $k = k_z \boldsymbol{z_0} + k_y \boldsymbol{y_0}$ (k_y being the transversal wavenumber) propagate. In the quantum domain, such a heterostructure is commonly described by the 4–band Kane's model (1.17), where these bands correspond to conduction electrons (symmetry Γ_6), light and heavy holes (symmetry Γ_8) and split–off holes (symmetry Γ_7). Then using the approximations suggested in [71], which involves dropping the free space terms for the Γ_7 and Γ_8 bands, the spin states of the conduction electrons remain degenerated even at oblique incidence, and are described by a scalar equation for the wave–function, that is evaluated from Eq. (1.17)

$$\left[-\frac{\hbar^2}{2m} \frac{\partial^2}{\partial z^2} + \frac{\hbar^2}{2m} k_y^2 + E_{\Gamma_6} - E \right] f_c(z) = 0 \tag{3.1}$$

where

$$\frac{1}{m} = \frac{2P^2}{3}\left(\frac{2}{E - E_{\Gamma_8}} + \frac{1}{E - E_{\Gamma_7}}\right) \tag{3.2}$$

is the inverse of the mass of the electron inside the material (1.19) and E is the energy of the electron. Parameter P, known as the Kane's parameter, does not depend on energy, is well defined for commonly used semiconductors, and can be obtained from experiments or from microscopic calculations. Following [49], the equation (3.1) is rewritten in matrix form

$$\frac{\partial}{\partial z}\begin{bmatrix} f_{\mathrm{c}} \\ -\mathrm{i}\frac{\hbar}{m}\frac{\partial f_{\mathrm{c}}}{\partial z} \end{bmatrix} = \begin{bmatrix} 0 & \frac{\mathrm{i}m}{\hbar} \\ \frac{2\mathrm{i}\left(E - E_{\Gamma_6} - \frac{\hbar^2}{2m}k_y^2\right)}{\hbar} & 0 \end{bmatrix} \begin{bmatrix} f_{\mathrm{c}} \\ \frac{-\mathrm{i}\hbar}{m}\frac{\partial f_{\mathrm{c}}}{\partial z} \end{bmatrix} \tag{3.3}$$

and supplemented by boundary conditions by the continuity of f_{c} and $\left(\partial f_{\mathrm{c}}/\partial z\right)/m$ at all heterostructure boundaries.

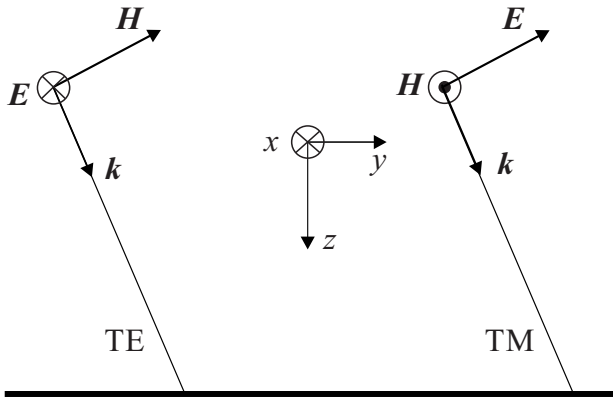

Figure 3.1: Geometry of a transverse electric (TE) wave and a transverse magnetic (TM) wave.

Due to the vector nature of electromagnetic fields, the propagation of electromagnetic plane waves in an isotropic medium, unlike ballistic electrons, depends on polarization. For simplicity and clarity is considered that the TE wave is characterized by k_y, k_z, E_x,H_y, H_z, $\frac{\partial}{\partial x} \to 0$, $\frac{\partial}{\partial y} \to \mathrm{i}k_y$ and TM wave is defined as k_y, k_z, E_y, E_z, H_x, $\frac{\partial}{\partial x} \to 0$, $\frac{\partial}{\partial y} \to \mathrm{i}k_y$ (see Fig. 3.1). The propagation of TE and TM waves in an isotropic material is described by Maxwell's equations that can be written as

$$\frac{\partial}{\partial z}\begin{bmatrix} E_x \\ \frac{-\mathrm{i}}{\omega\mu}\frac{\partial E_x}{\partial z} \end{bmatrix} = \begin{bmatrix} 0 & \mathrm{i}\omega\mu \\ \mathrm{i}\omega\varepsilon\left(1 - \frac{k_y^2}{\omega^2\varepsilon\mu}\right) & 0 \end{bmatrix} \begin{bmatrix} E_x \\ \frac{-\mathrm{i}}{\omega\mu}\frac{\partial E_x}{\partial z} \end{bmatrix} \tag{3.4}$$

for the TE wave and

$$\frac{\partial}{\partial z}\begin{bmatrix} H_x \\ \frac{-\mathrm{i}}{\omega\varepsilon}\frac{\partial H_x}{\partial z} \end{bmatrix} = \begin{bmatrix} 0 & \mathrm{i}\omega\varepsilon \\ \mathrm{i}\omega\mu\left(1-\frac{k_y^2}{\omega^2\varepsilon\mu}\right) & 0 \end{bmatrix}\begin{bmatrix} H_x \\ \frac{-\mathrm{i}}{\omega\varepsilon}\frac{\partial H_x}{\partial z} \end{bmatrix} \tag{3.5}$$

for TM wave. The boundary conditions (2.7) in this case demand the continuity of E_x, H_x, $\left(\partial E_x/\partial z\right)/\mu$ and $\left(\partial H_x/\partial z\right)/\varepsilon$.

By mutual comparison of (3.3) with (3.4) and (3.5), the analogy between electron waves and electromagnetic plane waves can be written as

Table 3.1: The analogy between the electron wave and plane electromagnetic waves.

Electron wave	**TE wave**	**TM wave**
f_c	E_x	H_x
m	μ	ϵ
$\Delta E = 2\left(E - E_{\Gamma_6}\right)$	ϵ	μ
$k^2 = m\Delta E/\hbar^2$	$\omega^2\varepsilon\mu$	$\omega^2\varepsilon\mu$

3.2 Design of a poor–man's lens

As was already mentioned, the perfect lens can be designed as a layered heterostructure of isotropic materials. The simplest design is defined as an isotropic slab of thickness d_lens with material constants ε_in and μ_in surrounded by another isotropic material with parameters ε_out and μ_out. If the materials are chosen [46] so that $\varepsilon_\mathrm{out} = -\varepsilon_\mathrm{in}$ and $\mu_\mathrm{out} = -\mu_\mathrm{in}$ the slab behaves as a perfect lens, which transfers all plane waves, including all evanescent harmonics, from the source plane at a distance d_source in front of the lens, to the image plane, which is situated at a distance d_image behind the lens, provided that the distances are chosen such that $k_z^\mathrm{out} d_\mathrm{source} + k_z^\mathrm{out} d_\mathrm{image} = k_z^\mathrm{in} d_\mathrm{lens}$.

Comparing the above mentioned conditions and the analogies from Tab. 3.1, it can be seen that the quantum analogy of the perfect lens is rather unlikely to exist. This is due to the fact that the mass m and ΔE are mutually bound by the material bandstructure. Therefore, these variables cannot be tuned separately, as is the case in electromagnetic metamaterials, in which ε, μ are usually connected to distinct elements. Fortunately, as shown in [46], if one is working in quasi–static conditions ($k_y \gg \omega\sqrt{\varepsilon\mu}$, i.e. in the near

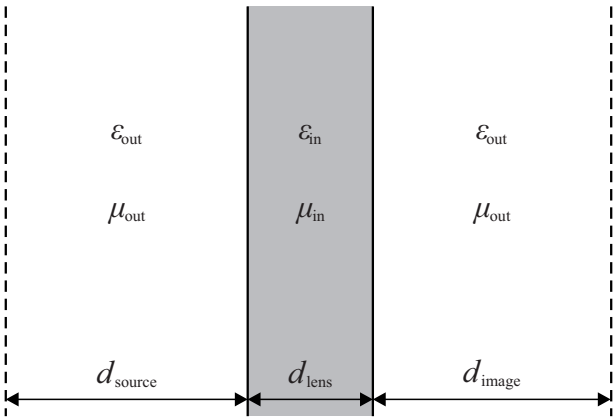

Figure 3.2: Sketch of a perfect lens for electromagnetic plane waves.

field) and is thus not interested in the propagative harmonics, then total transmission of the evanescent spectrum can be achieved by $\varepsilon_{\text{in}} = \text{any}$, $\mu_{\text{in}} = -\mu_{\text{out}}$ for TE waves and $\mu_{\text{in}} = \text{any}$, $\varepsilon_{\text{in}} = -\varepsilon_{\text{out}}$ for TM waves. This system is known as "the poor–man's lens". For an electron lens, this implies the use of a slab of $m < 0$ and $\Delta E = \text{any}$. The quasi–static regime in this case is given by $k_y \gg k = \sqrt{m\Delta E/\hbar^2}$. In order to put the above–stated conditions on solid grounds, the transmission and reflection coefficient of the lens is written as

$$T = \frac{4Y_{\text{in}}Y_{\text{out}}\mathrm{e}^{\mathrm{i}k_z^{\text{out}}d_{\text{image}}}e^{\mathrm{i}k_z^{\text{out}}d_{\text{source}}}}{\left(Y_{\text{in}}+Y_{\text{out}}\right)^2\mathrm{e}^{\mathrm{i}k_z^{\text{in}}d_{\text{lens}}}-\left(Y_{\text{in}}-Y_{\text{out}}\right)^2\mathrm{e}^{\mathrm{i}k_z^{\text{in}}d_{\text{lens}}}} \tag{3.6}$$

$$R = \frac{\left(Y_{\text{in}}^2+Y_{\text{out}}^2\right)\left(\mathrm{e}^{\mathrm{i}k_z^{\text{in}}d_{\text{lens}}}-\mathrm{e}^{-\mathrm{i}k_z^{\text{in}}d_{\text{lens}}}\right)\mathrm{e}^{2\mathrm{i}k_z^{\text{out}}d_{\text{source}}}}{\left(Y_{\text{in}}+Y_{\text{out}}\right)^2\mathrm{e}^{\mathrm{i}k_z^{\text{in}}d_{\text{lens}}}-\left(Y_{\text{in}}-Y_{\text{out}}\right)^2\mathrm{e}^{\mathrm{i}k_z^{\text{in}}d_{\text{lens}}}}, \tag{3.7}$$

where $k_z^2 = k^2 - k_y^2$ and $Y = k_z/m$. Clearly, in the case of the perfect lens ($\Delta E_{\text{out}} = -\Delta E_{\text{in}}$, $m_{\text{out}} = -m_{\text{in}}$, $d_{\text{source}} + d_{\text{image}} = d_{\text{lens}}$) there is $k_z^{\text{in}} = k_z^{\text{out}}$, $Y_{\text{in}} = -Y_{\text{out}}$ and thus $T = 1$ and $R = 0$, irrespective of k_y. The case of the poor–man's lens is a little more tricky. Assume that the waves are generated by a source at $z < 0$. For $k_y > k$ the physicality of the solution (wave decays in the direction of propagation) demands $k_z = \mathrm{i}\alpha$ with $\alpha > 0$. Assume further that $m_{\text{out}} = -m_{\text{in}}$ and $d_{\text{source}} + d_{\text{image}} = d_{\text{lens}}$. Two limits of (3.7) are then of interest. First, for $k_y \gg k$ but $\|k_z d_{\text{lens}}\| \ll 1$ there is $k_z^{\text{in}} \to k_z^{\text{out}}$, $Y_{\text{in}} \to -Y_{\text{out}}$ and $T \to 1$, $R \to 0$. The second limit is $k_y \to \text{inf}$ with $\Delta E_{\text{out}} \neq \Delta E_{\text{in}}$. In this case, (3.7),(3.9)

goes to

$$T \approx -\left(\frac{4\hbar^2 k_y^2}{m_{\text{in}}\left(\Delta E_{\text{in}} + \Delta E_{\text{out}}\right)}\right)^2 \mathrm{e}^{-2k_y d_{\text{lens}}} \approx 0 \tag{3.8}$$

$$R \approx \frac{4\hbar^2 k_y^2}{m_{\text{in}}\left(\Delta E_{\text{in}} + \Delta E_{\text{out}}\right)} \mathrm{e}^{-2k_y d_{\text{source}}} \approx 0. \tag{3.9}$$

In the case of the poor–man's lens, there thus clearly exist only a finite band of k_y for which $T \approx 1$. The bandwidth grows as the lens gets thinner and also as k gets smaller.

In summary, to create a poor–man's lens is necessary to fulfill several conditions:

- using the Kane's model assumes that the bulk edge eigenfunctions have to be the same (or very similar) at the interfaces throughout a heterostructure;
- the chosen materials have to fulfill aforementioned condition $m_{\text{in}} = -m_{\text{out}}$.

The first assumption can be achieved by using the same material in whole heterostructure. The second one is more difficult to achieve. The easiest way to fulfill the second condition is to find a material where the mass can change its value from positive to negative at given energy just using small static energy shift applied on the lens part of heterostructure. However this energy shift is not taken into account in the mode and therefore it has to be kept small to obtain meaningful results. Moreover the outer material needs to be propagative for $k_y = 0$. The suitable material, where this kind of behavior can be found, is material with so–called inverted bandstructure, in which the Γ_6 band edge is below the Γ_8 band edge. According to Kane's model, the negative effective mass means that $2/\left(E - E_{\Gamma_8}\right) < -1/\left(E - E_{\Gamma_7}\right)$. To stay in the region of validity of 4–band model, we always need to stay above the split–off band (which is the lowest from the 4 bands).

To design the poor–man's lens as it is proposed above, the mercury telluride (HgTe) is chosen for its specific properties - the inverted bandstructure. To use the Kane's model (3.1), (3.2) it was necessary to obtain parameter $2m_eP^2$ to determine normalized mass from (3.2), and the energies E_{Γ_6}, E_{Γ_7} and E_{Γ_8} for HgTe. The parameter $2m_eP^2$ was adjusted so that the curvatures of the bands were very similar as in the bandstructure obtained by local pseudopotential method (LPM) (see Appendix A). In the local pseudopotential method [76], [77], the Hamiltonian is divided into two part, one describes potential of zinc-blend structure, i.e. atoms, which are in the Brillouin zone, are approximated by form factors and structure factors [78] and the second describes the spin orbit splitting. To specify the zinc–blend structure were used 137 general reciprocal lattice vectors. Fig.3.3 shows the

comparison of these methods in several cases. As can be seen, behavior of bandstructures obtained from Kane's model and LPM is the same or very similar for small k_z. For higher k_z, Kane's model ceases to describe the bandstructure of the material for the small number of bands used in calculating (Fig.3.3a-b). In cases when $k_y \neq 0$ there occurs an expansion of the bandgaps and the spin states cease to be degenerate (Fig.3.3c-d), which can be seen in LPM results. In the Kane's model within our approximation, the spin states are degenerated in all cases.

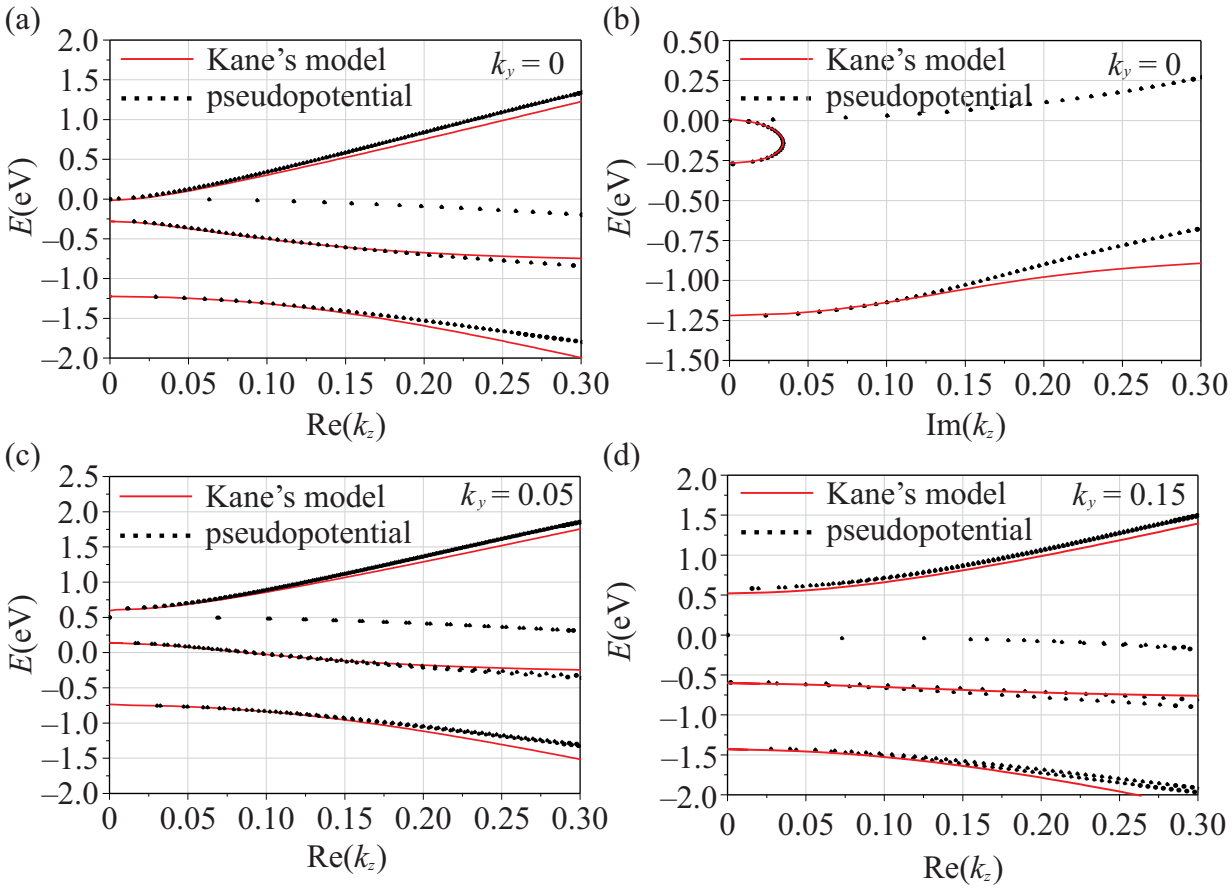

Figure 3.3: The comparison of bandstructure computed by the Kane's model (solid) and using the local pseudopotential method A (dot) in different cases.

From the Fig.3.4a it is obvious that the value of effective mass can be changed from negative to positive by using small energy shift. Actually the absolute values of normalized mass, which is computed from normalized equation (3.2) for HgTe, are very similar for its linear character around the energy E_{Γ_8}. This ensures that the energy shift, created by applied voltage, causes the effective mass in a given space changes from positive to

negative. Small energy shift does not cause major changes of bandstructure and therefore the boundary conditions at the interfaces are satisfied. To design the quantum poor–

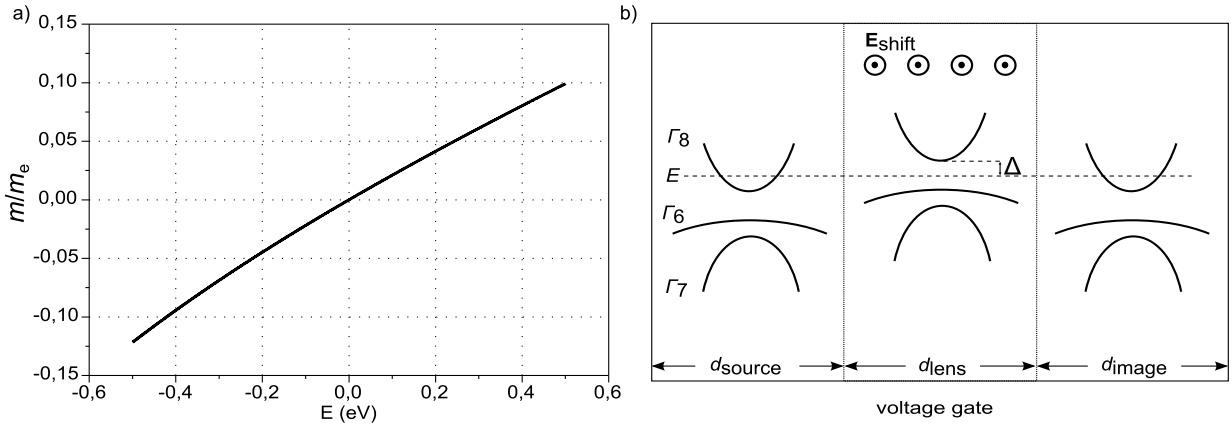

Figure 3.4: (a) Dependence of the normalized mass on the energy of electron around the E_{Γ_8}. (b) Sketch of the poor–man's lens (illustrates a top view). The electrodes are on the whole surface. The lens is created by applied voltage, which produces the homogeneous electric field that shifted the bandstructure of 2Δ.

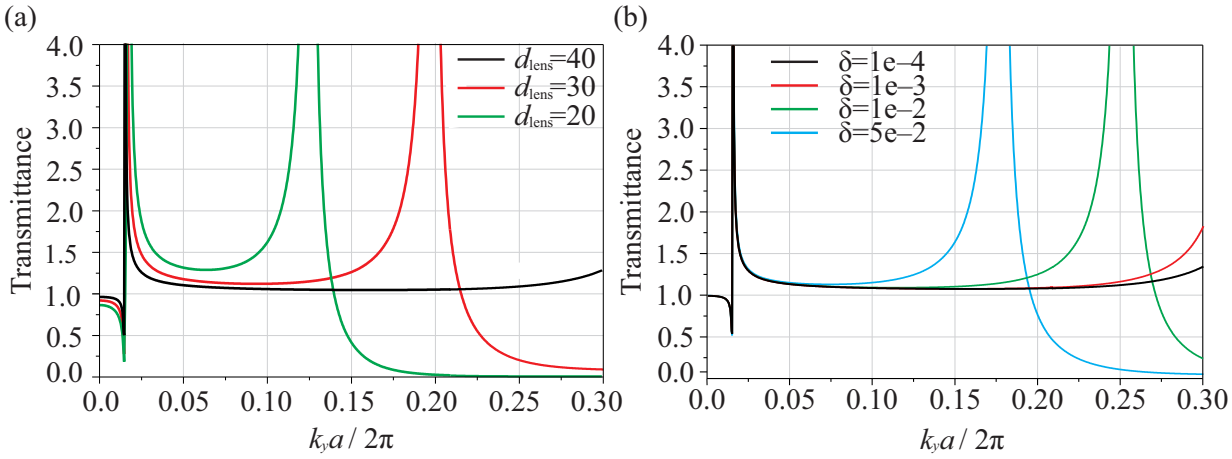

Figure 3.5: (a) The transmission coefficient as a function of k_y. The wavenumber is normalized to $2\pi/a$ and distances to $a/(2\pi)$, where a is the lattice constant. (b) The transmission coefficient depends on $\delta = 2(m_{out} + m_{in})/(m_{out} - m_{in})$. The transmission coefficient is computed for lens distance $d_{lens} = 20$.

man's lens, all requirements are fulfilled by using the HgTe. The proposed lens structure is depicted in Fig.3.4b. By applied voltage, the energy shift is achieved in the middle part

of the heterostructure. If the energy of an electron E is chosen as shown at Fig.3.4b, the energy shift caused the change of a sign of the mass, but not the value, because of linear character of the mass (Fig.3.4a). The transmission coefficient through this heterostructure is depicted in Fig.3.5a for several values of d_{lens}. The energy shift was intentionally chosen so that the masses slightly deviate from ideal situation in which $m_{\text{in}} = -m_{\text{out}}$. For this purpose it was chosen $2\,(m_{\text{out}} + m_{\text{in}})\,/\,(m_{\text{out}} - m_{\text{in}}) = -10^{-5}$. The curves in Fig.3.5b show how the lens is sensitive in this respect. The comparison of the figures 3.5a and 3.5b for the transmission coefficient shows that the transmission coefficient is more sensitive to lens distance d_{lens} than to differences between effective mass.

3.3 Verification of the poor–man's lens

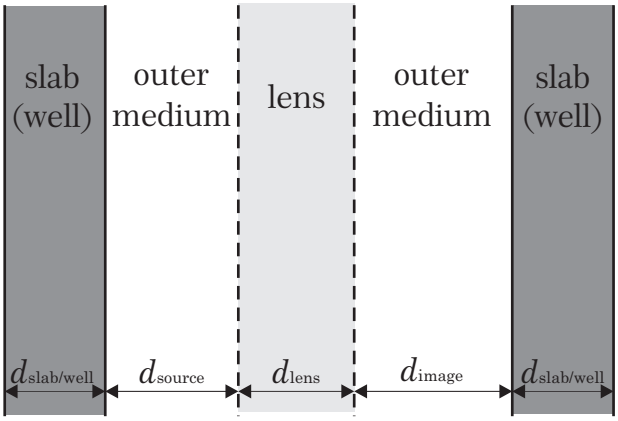

Figure 3.6: A sketch of the system used for verification.

For better understanding what happens due to the changes of the thickness of the poor–man's lens theoretical experiment has been proposed. The assumption is that the two quantum wells are perfectly bound just when the suitable perfect lens is put between them. For comparison the coupling of two dielectric slabs in electromagnetic case is shown in the first part of this chapter. In the second part, the poor–man's lens is verified.

The general system, which is used in following, is depicted on Fig.3.6. Quantum wells of thickness d_{well} are situated in infinite material. The distance between the quantum wells is $d_{\text{source}} + d_{\text{image}} + d_{\text{lens}}$.

3.3.1 Two Dielectric Slabs: Electromagnetic case

In the electromagnetic case, a quantum well can be considered as infinite slab of a thickness d_{well} with a high–valued permittivity $\varepsilon_r^{\text{well}}$ and permeability μ_r^{well} which is situated in another medium with a low–valued permittivity $\varepsilon_r^{\text{out}}$ and permeability μ_r^{out}. In these slabs can exist bound states which can be described in the same way as the eigenmodes of a dielectric waveguide [79]. These modes depend on a dimension of the dielectric waveguide and also on the material constants of used material. But the modes are not localized only in the waveguide, part of the field penetrate also into the outer medium. The penetration is defined by the ratio of the permittivity of the waveguide material and the permittivity of the outer material. If the difference between permittivities (permeabilities) is big, the modes are bound in the waveguide much stronger than in the case when the permittivities (permeabilities) are similar. The localization of the modes in the waveguide also depends on the order of the mode. The higher modes leak into the outer medium more than the lower.

In following cases, two infinite dielectric slabs of thickness d_{well} with relative permittivity $\varepsilon_r^{\text{well}} = 100$ and the relative permeability $\mu_r^{\text{well}} = 100$ are used. All dimensions are normalized to the thickness of the dielectric slab. To find an eigen wavenumber $k_0 = \sqrt{k_y^2 + k_z^2}$ of the system of two dielectric slabs, ABCD method was used [80].

3.3.1.1 Two dielectric slabs in vacuum

Firstly, the behavior of the coupling of two dielectric slabs situated in vacuum is discussed. The slabs are perfectly bound if they are connected. By this connection, the new, bigger dielectric slab arises which width is $2d_{\text{lens}}$. For this well, the first two bound states (eigenstates) characterized by wavenumbers are calculated. When the distance between quantum wells increases, the wavenumber of the first bound states changes its value and starts to approach to the value of the second bound state wavenumber. Exactly this mode determines how strongly the quantum waves are mutually bound. The difference between wavenumbers of the first two bound states is smaller, the quantum wells are bound weaker. When the value of the first mode wavenumber takes the value of the second one, the quantum wells become mutually independent, it appears the only one quantum wells is the entire space. In the case of the two dielectric slabs situated in vacuum, the slabs are mutually independent even when the distance between them is quite small, as is clear in Fig.3.7a (dot–line).

3.3.1.2 Two dielectric slabs bound by the perfect lens

In the case that the perfect lens is put between the two dielectric slabs, these slabs should have been bound perfectly independently on the distance between them. This hypothesis is based on the theory of the electromagnetic perfect lens [46]. The perfect lens is created by the material with the relative dielectric constant $\varepsilon_r^{\text{lens}} = -1$ and the relative permeability $\mu_r^{\text{lens}} = -1$. The width of the perfect lens d_{lens} increases with increasing distance between the slabs such that the condition $d_{\text{source}}k_z^{\text{out}} + d_{\text{image}}k_z^{\text{out}} = d_{\text{lens}}k_z^{\text{in}}$ is fulfilled. In Fig. 3.7a, the solid line represents the result of calculation of the bound state wavenumbers in the dielectric slabs, namely, dependence of the difference between the first two bound state wavenumbers of the quantum wells on the distance. As is seen, the difference between the wavenumbers is constant and the value of the difference is the same as in the case when the dielectric slabs are connected into one well. These findings mean that the quantum wells are still perfectly mutually bound independently on the distance between the slabs if the suitable perfect lens is used.

3.3.1.3 Two dielectric slabs bound by the poor–man's lens

The most important case for the comparison, is the case when the two dielectric slabs are bound by a poor–man's lens. As is mentioned in section 3.2, the poor–man's lens works only in quasi–static regime, i.e. $k_y >> k$ and only for evanescent harmonics. Both these conditions are fulfilled in our calculations. The quasi–static regime is guaranteed by high–valued transverse wavenumber k_y. The bound states are defined such that the wave is propagative in the slab but outside of the slab is evanescent. For perfect coupling of two slabs is needed that the field leaked from the first slab (evanescent harmonic) reaches into the second slab what the poor–man's lens is supposed to ensure. The poor–man's lens in our computation is created by material with the relative permittivity $\varepsilon_r^{\text{lens}} = 1$ and the relative permeability $\mu_r^{\text{lens}} = -1$. The dashed line in the Fig.3.7a shows that the poor–man's lens contributes significantly to coupling of two dielectric slabs, but the slabs are not bound perfectly. The difference of the bound state wavenumbers decreases with increasing distance, what corresponds with the results in section 3.2. Finally, when the distance between the quantum wells is 160 n.u. or longer, the slabs are not more mutually bound and they behave like there is no poor–man's lens, even like the only one quantum well is in the whole space.

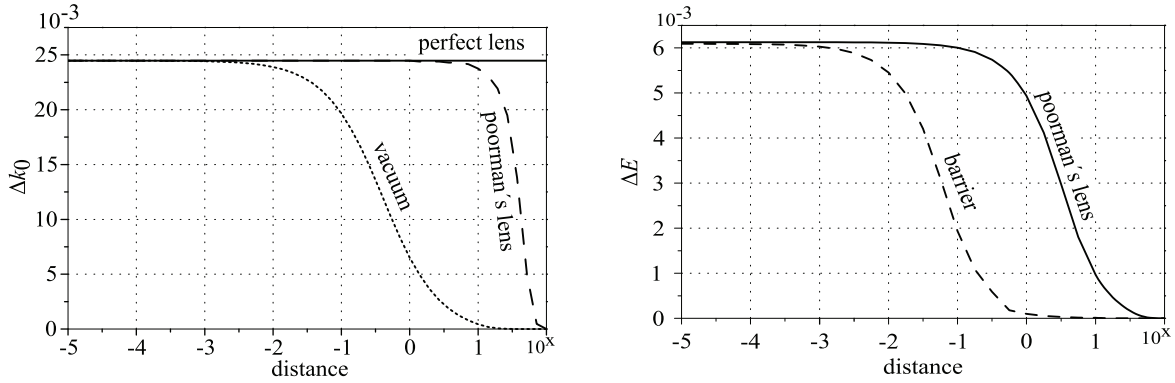

Figure 3.7: a) Dependence of difference between the first two eigenstates wavenumbers on a distance between two quantum wells when the quantum wells: are in vacuum (dotted), are bound by poor–man's lens (dashed), are bound by perfect lens (solid). b)Dependence of the difference between the energies represented the first two eigenstates on a distance between two quantum wells when the quantum wells: are separated by potential barrier (dashed), are bound by poor–man's lens (solid).

3.3.2 Two quantum wells: Electron case

In this part the quantum poor–man's lens is verified such that the coupling of two quantum wells separated by a barrier of different width is observed. The quantum well for an electron can be described as a finite potential well of width d_{well} [81]. Similarly to the previous case also potential well has bound states which can be obtained as a solution of time–independent Schrödinger equation 1.3. The resulting wave represents a probability function of the occurrence. Because of the finiteness of the potential well, the probability of the occurrence is non–zero also out of the well. The bound states of the finite potential well are the quantum analogy of aforementioned bound states in the electromagnetic case. To evaluate the behavior of two quantum wells when they are moving away from each other the same method as in previous case was used. In the calculations, HgTe was assumed as a medium. The potential wells were created by static energy shift of the bandstructure to give a potential barrier at the interfaces.

3.3.2.1 Two quantum wells in various distances

In quantum mechanics, the coupling of two potential wells means how big is the ability of the electron to tunnel from the first potential well to the second well. In the first case, the behavior of the two quantum wells created as two potential wells separated by potential

barrier of various width is investigated. In Fig. 3.7b - dashed line shows the dependence of the difference between two energies which represent 2 bound states on the width of the potential barrier, i.e. on the distance between these quantum wells. It is clearly seen that the behavior is the same as in the electromagnetic case, where the two dielectric slabs are situated in the vacuum. The quantum wells are mutually unbound even the distance between them is really small.

3.3.2.2 Two quantum wells bound by the quantum poor–man's lens

Finally the coupling of two quantum wells by a suitable poor–man's lens is examined. In this results a poor–man's lens is created as a slab of material surrounded by another material where the electron masses are defined $(m_{\mathrm{out}} + m_{\mathrm{in}}) / (m_{\mathrm{out}} - m_{\mathrm{in}}) \approx 5 \cdot 10^{-6}$ and dimensions are such that $d_{\mathrm{source}} k_z^{\mathrm{out}} + d_{\mathrm{image}} k_z^{\mathrm{out}} = d_{\mathrm{lens}} k_z^{\mathrm{in}}$. When the suitable poor–man's lens is used, the coupling of the quantum wells is stronger than in the case, when the the quantum wells are separated by potential barrier, as is seen in Fig. 3.7b - solid line. However, in the comparison with electromagnetic case of coupling of two dielectric slabs by poor–man's lens, the coupling is not so strong. As was shown in previous chapter, the quantum poor–man's lens is strongly dependent on the difference of the electron masses, thus the coupling of two quantum wells becomes weaker faster.

Chapter 4

A Core–shell Trap For Electrons

Previous chapter showed how to perfectly couple two potential wells, i.e., how achieve perfect tunneling of an electron from one potential well into another. This chapter will in contrary study how to trap an electron within the potential well. It may seem that such functionality is only achieved in an infinite potential well. It, however, turns out that there exists such quantum system that is described as a finite potential well but it has perfect bound states also known as stationary states.

The stationary states of a quantum system with a finite height potential well are commonly divided into bound states, which form a discrete spectrum, and unbound states which form a continuum [59]. Usually, the two classes of modes do not overlap: the energies of the bound states usually lie within a potential well, while the energies of unbound states lie above the potential well. Surprisingly, this property of a quantum system is not universal, as there are theoretical predictions of systems with bound state energies falling into the continuum, so–called bound states in the continuum – BICs. Pioneering work pointing out that bound states with energies in the continuum are exact solutions of the one–electron Schrödinger equation for specific potentials was presented by von Neumann and Wigner in 1929 [16]. The original formulation of von Neumann and Wigner has been reworked and even extended to a two–electron wave function [17], still bearing the sign of BICs. More recently, it has been proposed that the BICs can be decoupled from all continuum states also by virtue of symmetry [18, 19, 20].

Alongside the paradigm introduced above, the so–called "resonant states" in quantum systems have been discovered [82]. These represent a different approach for achieving "bound" states (resonances) with energies lying above the continuum threshold. These narrow–width resonances were proposed to exist as metastable states trapped by a large

potential barrier, or as quasi–bound states in closed channels of a system with weakly coupled channels [83, 18, 19, 20]. Strictly speaking, however, these states are not truly bound, as they are in fact localized states with a finite lifetime constructed from continuum states. Their appearance is however very close to true BICs.

The experiment closest to observing BICs was carried out by Capasso in 1992 [84]. The “bound state", albeit with energy above the potential barrier, was *de facto* a defect mode achieved by Bragg reflections in the periodic system of potential wells [85]. Another similar experiment, where the bound states were coupled to the continuum, was the case of (Ga,In)(As,N)/(Al,Ga)As quantum wells done by Albo et al [21].

Until recently, all the known realizations of BIC resonators required infinitely extended material profiles, e.g. a photonic crystal. Truncation of the material profile leads to imperfect localization and to finite oscillation lifetimes. Importantly, however, it was shown for the first time in [25] that spatially unbounded resonators are not required to have BICs, and that, under some strict conditions, volume plasmons may enable the formation of BICs in open cavities of finite size.

In this chapter a semiconductor heterostructure supporting BICs is proposed, although it is characterized by a potential well of finite height. Inspired by [25] and using an electron–light wave analogy, we show that an electron can be trapped with an infinite lifetime within a spherical core–shell heterostructure when the electron dispersive mass in the shell is precisely zero and the radius of the core is precisely tuned. All results are based on an effective medium approximation [69] described in Chap. 1.2.

4.1 Analogy between electron waves and light waves for spherical systems

The idea to trap an electron inside a core-shell heterostructure invites us to look at the electron–light–wave analogy also for spherical system. Rather straightforward solution can be found for electron that is described by a spherical wave. In such a case, one can look for a solution of Eq. (1.23) of the form $\psi_{\text{eff}}(\boldsymbol{r}) = R_l(r) P_l(\cos\theta)$, where $P_l(\cos\theta)$ represents a Legendre polynomial of order l [86]. To ensure that the wave function $\psi_{\text{eff}}(\boldsymbol{r})$ follows the relevant physics at the interfaces of the layers, equation (1.22) is further complemented with boundary conditions, i.e. with the continuity of ψ_{eff} and $\partial_{\text{n}}\psi_{\text{eff}}/m$ at each boundary, where $\partial_{\text{n}} = \partial/\partial\text{n}$ and n represents the direction normal to the boundary surface [68, 55].

For convenience, we introduce the function $\tilde{\psi_{\text{eff}}}(\boldsymbol{r}) = \psi_{\text{eff}}(\boldsymbol{r})/m$, which proves useful for handling the limit $m \to 0$ ($E = E_{\Gamma_8}$), which will be discussed later. Note that the boundary conditions satisfied by $\tilde{\psi_{\text{eff}}}$ are the continuity of $m\tilde{\psi_{\text{eff}}}$ and the continuity of $\partial_{\text{n}}\tilde{\psi_{\text{eff}}}$.

Assuming all aforementioned it is straightforward to show [86] that the time–independent Schrödinger equation reduces to

$$\frac{1}{r^2}\frac{\partial}{\partial r}\left[r^2\frac{\partial \tilde{R}_l}{\partial r}\right] + \left[\frac{2m}{\hbar^2}\left(E - E_{\Gamma_6}\right) - l\left(l+1\right)\frac{1}{r^2}\right]\tilde{R}_l = 0. \tag{4.1}$$

Due to the orthogonality of the spherical harmonics and the spherical symmetry of the system, the boundary conditions for $\tilde{\psi_{\text{eff}}}(\boldsymbol{r})$ reduces to the continuity of $m\tilde{R}_l(r)$ and $\partial_r\tilde{R}_l(r)$ at each heterostructure boundary.

Unlike an electron in a crystalline heterostructure, a light bound mode in an electromagnetic heterostructure is described by a vector wave equation. In general, the vector wave equation does not reduce to three uncoupled scalar equations, so there is no immediate analogy between the light case and the electron wave case. In the case of spherical coordinates [86], the electromagnetic fields can fortunately be separated into transverse electric radial TE^r waves and transverse magnetic radial TM^r waves (transverse with respect to the radial direction) [87]. The TE^r and the TM^r waves can be derived from a single component of the electric vector potential $\boldsymbol{F} = \hat{\boldsymbol{r}}F_r$, and the TM^r waves can be derived from a single component of the magnetic vector potential $\boldsymbol{A} = \hat{\boldsymbol{r}}A_r$, so that the vector wave equation reduces to a scalar wave equation [87, p.553-557].

$$\left(\Delta + k^2\right)\frac{F_r}{r} = 0, \tag{4.2a}$$

$$\left(\Delta + k^2\right)\frac{A_r}{r} = 0. \tag{4.2b}$$

By analogy with the electronic case, we introduce auxiliary functions $\tilde{F}_r = F_r/\mu r$ and $\tilde{A}_r = A_r/\varepsilon r$, so that the wave equations (4.2a) and (4.2b) are further complemented by boundary conditions that impose the continuity of $\mu\tilde{F}_r$ and $\partial_r\tilde{F}_r$ for the TE^r waves, and the continuity of $\varepsilon\tilde{A}_r$ and $\partial_r\tilde{A}_r$ for the TM^r waves, where ε, μ are the permittivity and the permeability, respectively.

By comparing of (1.17) and (4.2a), (4.2b) and the corresponding boundary conditions, a direct analogy between the semiconductor and the electromagnetic cases is obtained, see Table 4.1.

Table 4.1 also reveals that the presented electron–light analogy for spherical waves is very similar to that for plane waves [53, 88, 89, 50].

Table 4.1: The analogy between an electron wave and electromagnetic waves.

Electron wave	**TE wave**	**TM wave**
$\tilde{\psi}_{\text{eff}} = \psi_{\text{eff}}/m$	$\tilde{F}_r = F_r/\mu r$	$\tilde{A}_r = A_r/\varepsilon r$
m	μ	ε
$2\left(E - E_{\Gamma_6}\right)$	ε	μ
$k^2 = \dfrac{2m\left(E - E_{\Gamma_6}\right)}{\hbar^2}$	$\omega^2\varepsilon\mu$	$\omega^2\varepsilon\mu$
$\Delta f + k^2 f = 0\ ,\ f = \left\{\tilde{\psi}_{\text{eff}}, \tilde{F}_r, \tilde{A}_r\right\}$		
continuity of		
$m\tilde{\psi}_{\text{eff}}$ $\partial_r\tilde{\psi}_{\text{eff}}$	$\mu\tilde{F}_r$ $\partial_r\tilde{F}_r$	$\varepsilon\tilde{A}_r$ $\partial_r\tilde{A}_r$

4.2 The embedded eigenstate

The idea of a trapped electron is inspired by the electromagnetic case [25], where it was shown that electromagnetic modes can under certain conditions be bound with infinite lifetimes in a core–shell nanoparticle. Particularly, the TM^r modes can be bound in the inner region of a core–shell nanostructure when the permittivity of the shell is zero–valued, $\varepsilon_{\text{shell}} = 0$, and the radius of the core has a precise value. In such the case, the shell has infinite transverse wave impedance and behaves, for this particular mode of oscillation, as a perfect magnetic conductor (PMC).

Applying the analogy described in the previous section, we see that an electron may be trapped in the core of a spherical heterostructure with an energy such that the dispersive mass of the shell vanishes. From Eq. (1.19) the condition $m = 0$ is satisfied for an energy such that $E = E^{(2)}_{\Gamma_8}$, i.e. at the edge of the valence (with p–type symmetry) band. In what follows, we will show that a semiconductor with a zero–valued dispersive mass may, indeed, effectively behave as an infinite barrier for the electron, and enables the emergence of a spatially localized stationary state embedded within the continuum. The geometry of the open quantum resonator is sketched in Fig. 4.1. This design is based on the ternary compound $\text{Hg}_{1-x}\text{Cd}_x\text{Te}$ with x being the mole fraction of cadmium [90]. This ternary compound is used mainly because of its favorable valence band offset values and due to the nearly perfect lattice matching between HgTe and CdTe.

In our design, both the core ($\text{Hg}_{0.9}\text{Cd}_{0.1}\text{Te}$) and the shell (HgTe) have inverted band-structures with the Γ_8 bands lying above the Γ_6 bands (Fig. 4.1), and the core and the

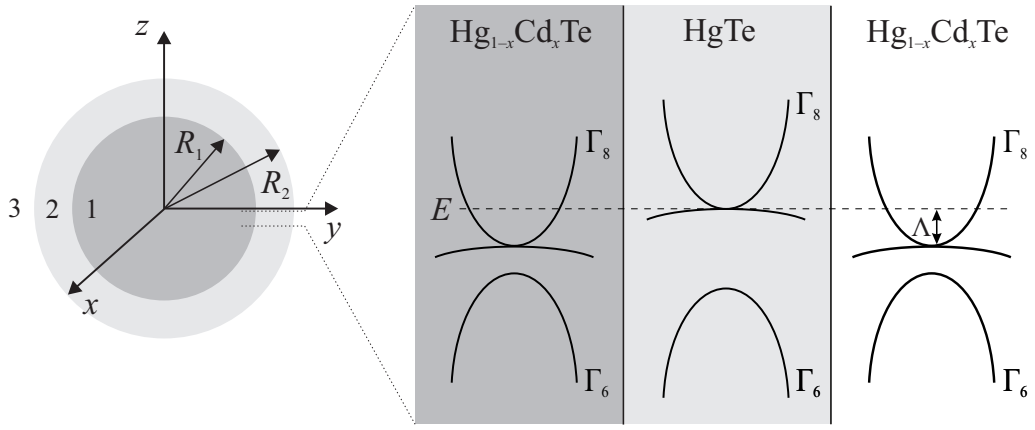

Figure 4.1: (left) A sketch of an open core–shell resonator for electrons consisting of a core with radius R_1 and a shell of width $R_2 - R_1$. The core–shell structure is surrounded by an infinite background material. (right) A sketch of the energy bandstructures of the heterostructure. The energy level associated with the embedded energy state is represented by a dashed horizontal line, and corresponds to the edge of the valence (Γ_8) band of HgTe. Number 1 denotes the core, number 2 denotes the shell, and number 3 denotes the background. Note that the considered semiconductor compounds have an inverted bandstructure, such that the order of the valence band Γ_8 and of the conduction band Γ_6 is reversed.

background materials are assumed to be identical. The fact that the semiconductor compounds have inverted bandstructures, and thus a negative dispersive mass within the band gap, does not play any role in the context of the emergence bound states embedded in the continuum. In principle, BICs can also be supported by other semiconductors with regular bandstructure. The band edge energies are calculated from the width of the band gap $E_{\rm g} = E_{\Gamma_6} - E_{\Gamma_8}$ and from the split–off energy $\Delta = E_{\Gamma_8} - E_{\Gamma_7}$. Energy $E_{\rm g}$ is computed from the Hansen's formula [90], considering zero temperature. The split–off energy is taken as $\Delta = 0.93$ eV [91]. The valence band offset between HgTe and $Hg_{1-x}Cd_xTe$ (see Fig. 4.1) is evaluated as $\Lambda = 0.35x$ eV [92]. The Kane's parameter P is given by the relation $2P^2 m_e/\hbar^2 = 18 + 3x$ eV [93]. Next, we formally demonstrate that Eq. (4.1) supports a bound state when $E = E^{(2)}_{\Gamma_8}$, i.e. when $m_2 = 0$ in the shell. Note that the energy level $E = E^{(2)}_{\Gamma_8}$ lies within the continuous energy spectrum of the background and core regions (Fig. 4.1), so the wavenumber $k_1 = \sqrt{2m_1\left(E - E^{(1)}_{\Gamma_6}\right)/\hbar^2}$ in the core and background regions is real–valued. Under the assumption that $m_2 = 0$ in the shell, and

that the wave function vanishes in the background region, the solution of the radial part of the Schrödinger equation (4.1) can be written in the form [86]

$$\tilde{R}_n(r) = N_0 \begin{cases} j_n(k_1 r) & r < R_1 \\ A_n (k_1 r)^n + B_n (k_1 r)^{-n-1} & R_1 < r < R_2 \\ 0 & r > R_2 \end{cases} \tag{4.3}$$

where N_0 is a normalization constant. The unknown coefficients A_n and B_n are determined by the boundary conditions, which require the continuity of $m\tilde{R}(r)$ and $\partial\tilde{R}(r)$ at the two interfaces. The continuity of $\partial\tilde{R}(r)$ implies that coefficients A_n and B_n are related as

$$A_n = \frac{(k_1 R_1)^{1-n}}{n} j_n'(k_1 R_1) \left[1 - \left(\frac{R_2}{R_1} \right)^{2n+1} \right]^{-1}$$

and

$$B_n = A_n \frac{n}{n+1} (k_1 R_2)^{2n+1}$$

where $j_n'(x) = \mathrm{d}j_n(x)/\mathrm{d}(x)$.

The continuity of $m\tilde{R}(r)$ imposes that the inner radius must satisfy:

$$j_n(k_1 R_1) = 0 \tag{4.4}$$

This condition shows that in order to have an embedded energy eigenvalue the radius of the core region must be chosen precisely. For $n = 1$ (dipole–type symmetry) this condition implies that the smallest possible radius for the core is $R_{1,\mathrm{res}} \approx 4.49/k_1$. This analysis confirms the hypothesis that the electron can be trapped in the core of the semiconductor heterostructure if the dispersive mass of the shell is zero–valued and the radius of the core has a very specific value.

It is important to highlight that:

- In the ideal case of $m_2 = 0$, the resonance condition is independent of the shell thickness.

- For $n = 0$, the calculated coefficients A_n and B_n are singular, and hence a wave function with monopole (s–type orbital) symmetry cannot be trapped within the core. This important result implies that our resonator is penetrable by waves with monopole symmetry, i.e. a semiconductor with a zero–valued dispersive mass behaves as an infinite barrier only for waves with a nonzero azimuthal quantum number. Thus, the core–shell heterostructure is generally open to electron waves. This is similar to

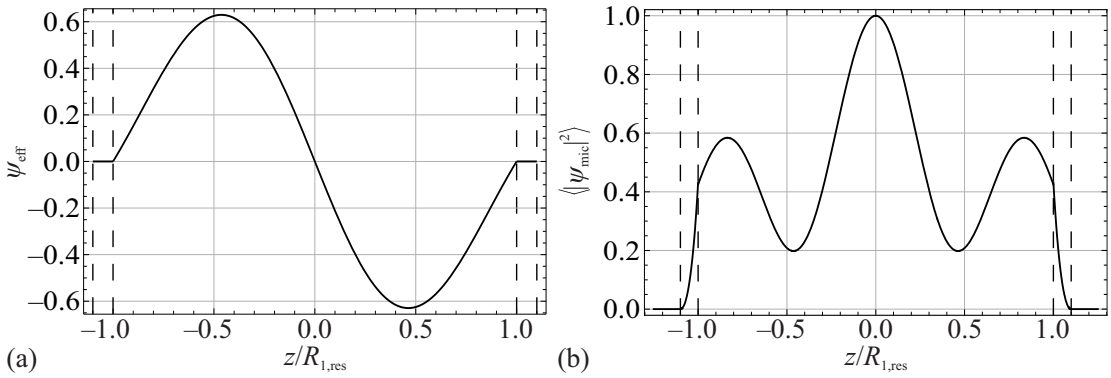

Figure 4.2: (a) The macroscopic wave function ψ and (b) the spatial average probability density $\langle|\psi|^2\rangle$ (normalized to the peak value) of the trapped electron as a function of the normalized z–coordinate.

the electromagnetic case, where the TM^r wave may be bound to the core by a shell made of permittivity near zero (ENZ) material, with the shell being penetrable by TE^r waves [25].

- The trapped modes are degenerate, because for each n there are in total $2n + 1$ spherical harmonics differing only in the magnetic quantum number [86].

To illustrate the proposed theory, a semiconductor heterostructure with an HgTe shell is considered. The $Hg_{1-x}Cd_xTe$ core has mole fraction $x = 0.1$ and radius $R_1 = R_{1,\text{res}} \approx 4.49/k_1 \sim 65a$, where $a = 0.65$ nm is the lattice constant of the considered bulk semiconductor alloys. The radius of the shell is $R_2 = 1.1R_{1,\text{res}}$. The trapped electron state has dipole–type symmetry ($n = 1$).

The calculated radius dependence of the "macroscopic" wave function ψ and the corresponding averaged probability density $\langle|\psi|^2\rangle$ for $\theta = \pi$ are depicted in Fig. 4.2. Note that from Eq. (1.22) in each layer $\langle|\psi|^2\rangle$ can be written in terms of $\tilde{\psi}$ as follows:

$$\langle|\psi|^2\rangle = m^2\left|\tilde{\psi}_{\text{eff}}\right|^2 + \hbar^2\frac{\partial m}{\partial E}\left\|\nabla\tilde{\psi}_{\text{eff}}\right\|^2. \tag{4.5}$$

To obtain the formula presented above, $\partial V_{\text{eff}}/\partial E = 0$ was used. It is interesting to note that for both semiconductor alloys $m \approx (E - E_{\Gamma_8})/2v_p^2$ in the energy range of interest, with $v_p^2 = 2P^2/3\hbar^2$ [54]. The parameter v_p has unities of velocity. Thus $\partial m/\partial E \approx 1/2v_p^2$, which is approximately the same in both the core and the shell. Figure 4.2a shows that the "macroscopic" electron wave function is entirely confined within the core, i.e. ψ_{eff} is identically zero not only outside the core–shell resonator, but also in the shell itself.

However, as is shown in Fig. 4.2b, the average probability density is non–zero in the shell. This means that the microscopic wave function (ψ) has strong fluctuations on the scale of the unit cell of the HgTe shell, so that its macroscopic spatial average vanishes in the shell, while the corresponding probability density function is non–zero. The fact that the probability of finding the electron in the shell is non–zero is consistent with the electromagnetic case, for which the electromagnetic energy stored in the permittivity near zero (ENZ) shell is non–zero. Thus, a zero dispersive mass, $m_2 = 0$, and a non–zero azimuthal quantum number, imply that the shell behaves as an infinite height potential barrier that blocks the electron tunneling out of the resonator.

It is relevant to note that in the electromagnetic case the light remains confined in the core region due to the screening provided by the (non–radiative) volume plasmons of the shell [25]. Interestingly, in the semiconductor case the role of the plasmons is played by the heavy–hole states of HgTe [94]. In our framework the heavy–hole states have a flat energy dispersion and occur precisely at the energy level wherein the dispersive mass vanishes.

4.3 Density of states

In order to further support the hypothesis of the emergence of the bound state in the continuum, the density of states in the background material has been evaluated as [60]

$$g\left(E\right) = \sum_{n} \frac{1}{\left(2\pi\right)^3} \int\limits_{E=E_{n\boldsymbol{k}}} \frac{1}{\left|\nabla_{\boldsymbol{k}} E_{n\boldsymbol{k}}\right|} \mathrm{d}S, \tag{4.6}$$

where the summation is over all bands. Accounting for a spin degeneration and realizing that the surfaces $E = E_{n\boldsymbol{k}}$ are spherical within the used effective medium model, the Eq. (4.6) can be simplified as

$$g\left(E\right) = \frac{1}{\pi^2} \frac{k^2}{\left|\hbar v_{\mathrm{g}}\right|}, \tag{4.7}$$

where

$$v_{\mathrm{g}} = \frac{1}{\hbar} \frac{\partial E}{\partial k} = v_P \frac{\sqrt{\left(E - E_{\Gamma_6}\right)\left(E - E_{\Gamma_8}\right)}}{\left(E - \left(E_{\Gamma_6} + E_{\Gamma_8}\right)/2\right)} \tag{4.8}$$

is the group velocity. It is important to note that Eq. (4.8) assumes the linear mass approximation $m \approx \left(E - E_{\Gamma_8}\right) / 2v_P^2$, which is valid in the vicinity of E_{Γ_8}.

From the dispersion of the energy stationary states it is possible to write the wave vector k as a function of the energy, so that one finally gets:

$$g\left(E\right) = \frac{\left[\left(E - E_{\Gamma_6}\right)\left(E - E_{\Gamma_8}\right)\right]^{1/2} \left|E - \left(E_{\Gamma_6} + E_{\Gamma_8}\right)/2\right|}{\pi^2 \hbar^3 v_P^3} \tag{4.9}$$

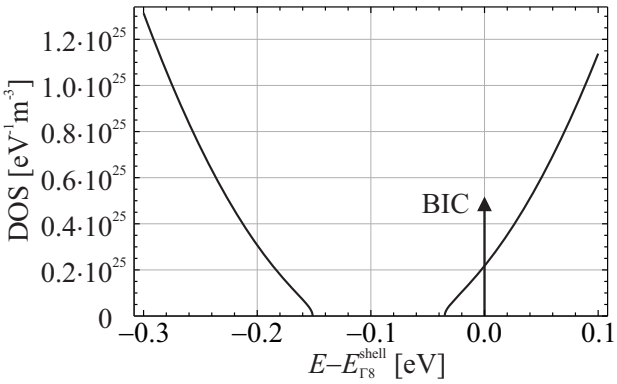

Figure 4.3: Density of states in the background medium. The vertical arrow represents the bound state in the continuum.

The density of states (4.7) is depicted in Fig. 4.3. It can be seen that it is non–zero at the energy $E = E_{\Gamma_8}^{(2)}$ associated with the BIC. This confirms that the discrete spectrum really overlaps the continuum spectrum. It is worth mentioning that the density of states of the background region is coincident with the density of states of the continuous spectrum of the structure. This is due to a one–to–one correspondence between the plane wave electronic states in the background unbounded region and the extended electronic states in the presence of the semiconductor heterostructure.

Note that the usual paradigm is that the bound states occur within the band gaps of the background material, different from Fig. 4.3. In the present example, it may be shown that there are no bound states in the band gap between the valence and conduction bands of the background region. This happens because the band gap of the shell overlaps the band gap of the background and of the core regions (Fig. 4.1).

4.4 The Trapping Lifetime for a Detuned Resonator

The previous section dealt with the ideal case, where the energy of the trapped electron is equal to the band edge energy - E_{Γ_8} - of the material in the shell, and the inner radius is perfectly tuned to the value $R_{1,\mathrm{res}}$ defined by Eq. (4.4). Such perfect tuning is however unrealistic, and it is interesting to characterize about the trapping lifetime when the inner radius R_1 is detuned.

In the detuned case, the solution of the radial equation (4.1) has to be searched in the

form

$$\tilde{R}(r) = \begin{cases} a_n j_n(k_1 r) & r < R_1 \\ b_n^{(1)} j_n(k_2 r) + b_n^{(2)} y_n(k_2 r) & R_1 < r < R_2 \\ c_n h_n^{(1)}(k_3 r) & r > R_2 \end{cases} \tag{4.10}$$

where j_n, y_n are the spherical Bessel functions of the first and second kind, respectively, $h_n^{(1)}$ is the spherical Hankel function of the first kind and $k_i = \sqrt{2m_i\left(E - E_{\Gamma_6}^{(i)}\right)/\hbar^2}$ is the wavenumber in the i-th layer. As in the previous section, the unknown coefficients a_n, $b_n^{(1)}$, $b_n^{(2)}$ and c_n are obtained from the boundary conditions discussed previously, which result in the following equation system

$$\begin{pmatrix} j_n(k_1R_1) & -\frac{m_2}{m_1}j_n(k_2R_1) & -\frac{m_2}{m_1}y_n(k_2R_1) & 0 \\ j'_n(k_1R_1) & -\frac{k_2}{k_1}j'_n(k_2R_1) & -\frac{k_2}{k_1}y'_n(k_2R_1) & 0 \\ 0 & \frac{m_2}{m_1}j_n(k_2R_2) & \frac{m_2}{m_1}y_n(k_2R_2) & -\frac{m_3}{m_1}h_n^{(1)}(k_3R_2) \\ 0 & \frac{k_2}{k_1}j'_n(k_2R_2) & \frac{k_2}{k_1}y'_n(k_2R_2) & -\frac{k_3}{k_1}h'^{(1)}_n(k_3R_2) \end{pmatrix} \begin{pmatrix} a_n \\ b_n^{(1)} \\ b_n^{(2)} \\ c_n \end{pmatrix} = 0 \tag{4.11}$$

In the detuned case, this homogeneous system (4.10) has a non–trivial solution only for complex energy values, $E = E_{\mathrm{re}} + iE_{\mathrm{im}}$, which correspond to the zeros of the matrix determinant. The imaginary part of the energy is associated with the decay time of the localized state, and non–zero E_{im} implies that the electron escapes from the resonator. The trapping lifetime can be defined as $\tau \sim \hbar/(-2E_{\mathrm{im}})$ [59]. The lifetime is independent of the origin of the energy scale. The trapping lifetime is shown in Fig. 4.4 as a function of relative detuning $R_1/R_{1,\mathrm{res}}$ for $R_2 = 1.1R_{1,\mathrm{res}}$. The calculation assumes that the core and the background are made of $Hg_{0.9}Cd_{0.1}Te$, and that the shell is HgTe.

4.5 Scattering Cross–section of the Core–shell Resonator

Since the resonator may support a state with an infinite lifetime, it is natural to ask if it can capture a free–electron propagating in the background region. To investigate this possibility, the scattering of a plane electron wave by the core–shell resonator will be studied.

Because of the angular symmetry of the resonator, it can be assumed without loss of generality that the plane wave propagates along the z-axis. This plane wave may be

decomposed into Legendre polynomials as [95]

$$\mathrm{e}^{\mathrm{i}k_3 z} = \sum_{n=0}^{\infty} \mathrm{i}^n \left(2n+1\right) j_n\left(kr\right) P_n\left(\cos\theta\right) \tag{4.12}$$

This decomposition allows us to write the normalized wave function as $\tilde{\psi} = \sum_0^\infty \tilde{\psi}_n$ with $\tilde{\psi}_n\left(r,\theta,\varphi\right) = \tilde{R}_n\left(r\right)\mathrm{i}^n\left(2n+1\right)P_n\left(\cos\theta\right)$ and

$$\tilde{R}_n\left(r\right) = \begin{cases} a_n j_n\left(k_1 r\right) & r < R_1 \\ b_n^{(1)} j_n\left(k_2 r\right) + b_n^{(2)} y_n\left(k_2 r\right) & R_1 < r < R_2 \\ c_n h_n^{(1)}\left(k_3 r\right) + j_n\left(k_3 r\right) & r > R_2 \end{cases} \tag{4.13}$$

The unknown coefficients are obtained by imposing the previously discussed boundary conditions at the interfaces. Figure 4.5a shows the first four ($n = 0, 1, 2, 3$) Mie scattering coefficients in the core region (a_n) as a function of the electron energy for a detuned resonator with $R_1 = 1.01 R_{1,\mathrm{res}}$. The curve corresponding to $n = 0$ (black line) confirms that the heterostructure is penetrable by an electron wave with monopole symmetry. This is in conformity with the claim in Sec. 4.2. However, the remaining curves show clearly that a_n ($n \geq 2$) vanishes whenever $E = E_{\mathrm{ideal}}$. For this energy, the shell region behaves as an infinite height barrier, and the incident electron wave is unable to reach the core region. The most relevant of these coefficients, a_1, which is associated with the trapped state, is

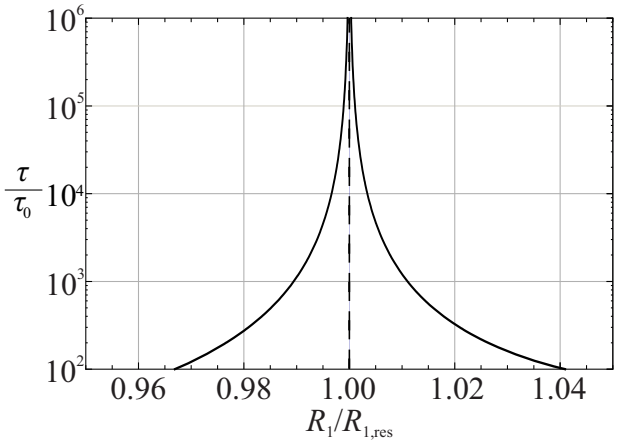

Figure 4.4: The trapping lifetime as a function of relative detuning $R_1/R_{1,\mathrm{res}}$. The trapping lifetime is normalized with respect to the time $\tau_0 = 2R_2/v_g = 0.11$ ps that the electron needs to pass the diameter of the core–shell resonator at the group velocity $v_g = v_p\sqrt{\left(E - E_{\Gamma_6}^{(3)}\right)\left(E - E_{\Gamma_8}^{(3)}\right)} / \left(E - \left(E_{\Gamma_6}^{(3)} - E_{\Gamma_8}^{(3)}\right)/2\right)$ in the background material.

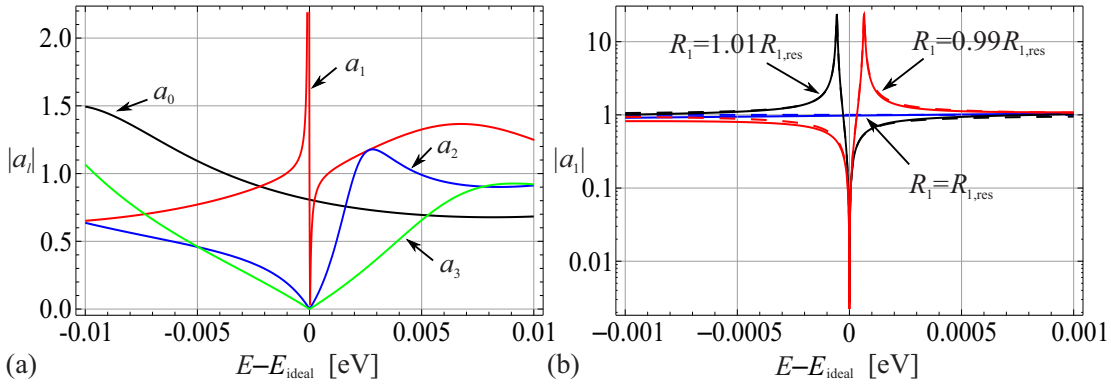

Figure 4.5: (a) Magnitude of the first four coefficients a_n $(n = 0, 1, 2, 3)$ as a function of relative energy detuning. The inner radius of the resonator is $R_1 = 1.01R_{1,\text{res}}$. (b) Magnitude of a_1 as a function of relative energy detuning. The inner radius is $R_1 = \{0.99, 1, 1.01\}\, R_{1,\text{res}}$. The full lines correspond to the exact solution while the dashed lines correspond to the approximation (4.14).

further studied in Fig. 4.5b for $R_1 \approx R_{1,\text{res}}$. In this case, our numerical simulations reveal that the approximation

$$a_1 \approx \frac{(E - E_{\text{ideal}})}{(E - E_{\text{actual}})} \mathrm{e}^{i\phi_0} \tag{4.14}$$

holds. In the above, E_{ideal} is the valence band edge energy E_{Γ_8} of HgTe for which the shell blocks an electron wave, E_{actual} is the complex valued resonance energy determined by the inner radius R_1 and which is calculated as is explained in Sect. 4.4, and ϕ_0 is some irrelevant phase factor. Notably, equation (4.14) and Fig. 4.5b reveal that in the limit case $R_1 \to R_{1,\text{res}}$ the zero associated with E_{ideal} cancels the pole corresponding to E_{actual}, and $|a_1| \to 1$. This contrasts with all the other a_n $(n \geq 2)$, which in the present example vanish identically for $E = E_{\text{ideal}}$, regardless of the radius R_1. This means that, due to the cancellation of a zero–pole, an incident wave with energy $E = E_{\text{ideal}}$ and dipole–symmetry *may* actually penetrates into the shell, in the case of a perfectly tuned resonator (see Fig. 4.5b, blue curve). Nevertheless, even though the resonator may support an infinite lifetime bound state and the free electron can penetrate into the core, it cannot be captured by the resonator. Indeed, the condition for having a trapped electron in the present problem is that $|a_1| \to \infty$ for some real–valued E. It may be checked that even though $|a_1|$ can have rather large values in our structure, it remains finite for any real–valued energy. We therefore conclude that, in the scenario studied here, the resonator is unable to capture the free electron.

This discussion may suggest that it is impossible to couple a free electron to the embedded bound state. However, that is not necessarily the case. For example, if the resonator is perturbed during a short time period (e.g. by applying a time–varying electric or magnetic field), the temporary detuning may allow the free electron to excite the bound state and be permanently captured after the perturbation is removed.

It is also interesting to characterize the scattering cross–section of the resonator. It is given by [96]

$$\sigma_{\mathrm{sc}} = \int_{\Omega} \frac{\left| \psi_{\mathrm{sc}} \dfrac{\partial \psi_{\mathrm{sc}}^*}{\partial r} - \psi_{\mathrm{sc}}^* \dfrac{\partial \psi_{\mathrm{sc}}}{\partial r} \right| r^2}{\left| \psi_{\mathrm{inc}} \nabla \psi_{\mathrm{inc}}^* - \psi_{\mathrm{inc}}^* \nabla \psi_{\mathrm{inc}} \right|} \mathrm{d}\Omega = \frac{4\pi}{k_1^2} \sum_n |c_n|^2 (2n+1) \tag{4.15}$$

where subscript “sc" stands for scattered, and subscript “inc" stands for incident. Figure 4.6a shows that for a perfectly tuned resonator with $R_1 = R_{1,\mathrm{res}}$ (blue curve), the scattering cross section does not exhibit any resonant features. This is consistent with the zero–pole cancellation discussed above. However, for a detuned inner radius R_1 there is a resonant response which indicates a strong interaction of the free–electron with the heterostructure because of temporary electron trapping. This behavior is also perceptible in Fig. 4.6b, where the scattering cross–section is represented for different energies of the incident electron.

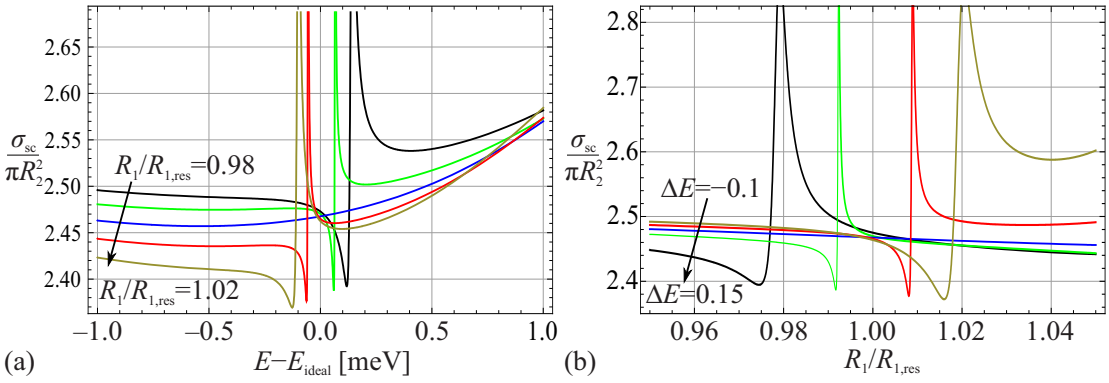

Figure 4.6: (a) Scattering cross section σ_{sc} as a function of relative energy detuning for $R_1/R_{1,\mathrm{res}} = 0.98, 0.99, 1, 1.01$ and 1.02. (b) Scattering cross section σ_{sc} as a function of the inner radius $R_1/R_{1,\mathrm{res}}$ for incident electron energy $E = E_{\mathrm{ideal}} + \Delta E$, where $\Delta E = \{0.15, 0.1, 0, -0.05, -0.1\}$ meV. In all calculation outer radius was taken as $R_2 = 1.1R_{1,\mathrm{res}}$.

4.6 Summary

It has been shown that a spherical semiconductor heterostructure may support bound states embedded within the continuum at an energy level where the shell region has a zero–valued dispersive mass. A realistic design of the heterostructure based on the $Hg_{1-x}Cd_xTe$ compound has been proposed. An in-depth analysis of the suggested heterostructure, based on the envelope function formalism, has been presented, showing the possibility to trap an electron within the resonator core. The trapping lifetime of a detuned heterostructure has also been characterized, and it has been shown that the heterostructure can trap the electron for a long time, even if there is slight detuning. Finally, we investigated the possibility of a free electron being captured by the semiconductor resonator. Notably, our analysis has revealed that, in the same manner as a trapped electron is unable to escape from the resonator, a free electron cannot be permanently captured by the resonator. Interestingly, the scattering cross section does not exhibit any resonant features for a perfectly tuned structure. This confirms that a free electron is unable to interact with the embedded bound energy eigenstate.

Chapter 5

Conclusion

5.1 Contribution of the thesis

The thesis provides an insight into the application of analogies between electromagnetic waves and ballistic electrons. It shows that the analogy can be used not only to understand of the behavior of an electron as a wave, but it can be used also to design a new semiconductor components. Here, the analogy was used to design so–called quantum metamaterials. Both ideas of design discussed in this work come from the electromagnetic world. Firstly it was shown that there can exist so–called poor–man's lens. It is a perfect lens for evanescent waves, i.e., it can transmit an oblique incident electron without any loss of energy. Such a lens is very similar to its electromagnetic counterpart. It is created as a layered heterostructure where each layer is suitably chosen. Then for a special range of energies the heterostructure behaves in a required way. Another design was based on an electromagnetic core–shell resonator. It was shown that such the resonator can trap an electromagnetic wave for infinite time, i.e., it can behave as a perfect resonator even for a frequency from the continues spectrum. In quantum mechanics such states are called bound states in continuum and their existence was proven in early years of quantum mechanics. However they have never been experimentally verified although a lot designs of system where BICs can be achieved. The proposed design in this work showed another system where BICs can be achieved. Advantage of the design is that it is created by a realistic materials, moreover the dimensions of the structure are technically achievable even in these days. On the other hand, the dimensions have to be precisely chosen, as was also shown in the chapter 4, which brings, together with high costs, a big disadvantage of the design.

5.1.1 Future directions

Theoretical developments described in this thesis shown that the concept of electron–light wave analogy is viable and can lead to novel designs. On the other hand, the study opened two questions which should be answered in future and are listed below.

- The first future work should aim at verification of proposed designs by some higher order methods , since the simplistic envelope function description could hide some important aspects of solid state physics. Several efforts in this direction have been already done using QuantumWise software that uses density function theory. Unfortunately, for QuantumWise, dimensions of proposed designs are too large to be manageable on regular computers.

- Examples of applications of electron–light–wave analogy mentioned in this text all work in the direction from electromagnetism to quantum mechanics. In future, it would be interesting to use the analogy in the opposite way. An interesting example can be to learn from so–called Empirical Pseudopotential Method (EMP) described in Appendix A and use a similar methodology for homogenization of electromagnetic metamaterials. EMP provides easily achievable description of complex medium using just a few parameters which can be obtained e.g. experiments. The idea is, in the future, create similar method in electromagnetism in which the medium will be described by an effective permittivity and effective permeability expressed in same manner as is effective potential. In such a case, there is assumption that there can exist finite number of coefficients needed for good description of a complex material, such as metamaterials.

Appendices

Appendix A

Empirical Pseudopotential Method

The empirical pseudopotential method (EPM) was developed in the 1960's [97, 98, 99] as a technique for solving the Schrödinger equation without knowing the exact potential experienced by an electron in the lattice. The core of the method is a knowledge that the observed physical properties of solids most of all dependent on valence electrons. Therefore, the EMP assumes that core electrons are tightly bound to the nucleus creating an ionic core not influencing much the macroscopic behaviour of the solid. Subsequently, the ionic core is replaced with a weaker pseudopotential, which acts on valence electrons described by a set of pseudo wave functions. Theoretical background of the pseudopotential theory can be started from the orthogonalized plane–wave (OPW) method in which the core and out–of–core wave function contributions are separated. Such wave can be written in form

$$\psi_{\boldsymbol{k}} = \varphi_{\boldsymbol{k}} + \sum_a c_a \varphi_a \tag{A.1}$$

where $\varphi_{\boldsymbol{k}}$ is a plane–wave–like function and φ_a in an atomic function and the sum goes through all occupied atomic shells. The coefficients c_a are chosen such that the function $\psi_{\boldsymbol{k}}$ is orthogonal to the atomic function φ_a. It is evident that the wave possesses following features: Out of the core the atomic functions φ_a are negligibly small and thus can be omitted, so $\psi_{\boldsymbol{k}} \approx \varphi_{\boldsymbol{k}}$. On the other hand, at the core, the atomic functions are considerable. It is easy to show that wave given by (A.1) is a solution of a one–electron Schrödinger equation

$$\left(\frac{p^2}{2m_e} + V^{\text{pseudo}} \right) \varphi_{\boldsymbol{k}}(\boldsymbol{r}) = E \varphi_{\boldsymbol{k}}(\boldsymbol{r}) \tag{A.2}$$

where pseudopotential V^{pseudo} is introduced. The pseudopotential is weaker than the real potential not showing any singularity in the ion core region. Due to the periodicity of

the pseudopotential V^{pseudo}, the function $\varphi_{\boldsymbol{k}}$ can be expressed according to the Bloch's theorem [60]

$$\varphi_{\boldsymbol{k}} = \sum_{c} \boldsymbol{G} \exp\left(\mathrm{i}\left(\boldsymbol{k}+\boldsymbol{G}\right)\cdot\boldsymbol{r}\right) \tag{A.3}$$

where $\boldsymbol{G}$ represents reciprocal lattice vectors. Substituting (A.3) into (A.2) gives

$$\begin{aligned}\frac{\hbar^2}{2m_e}\sum_{\boldsymbol{G}} c_{\boldsymbol{G}}\left|\boldsymbol{k}+\boldsymbol{G}\right|^2 \mathrm{e}^{(\mathrm{i}(\boldsymbol{k}+\boldsymbol{G})\cdot\boldsymbol{r})} + V^{\text{pseudo}}\left(\boldsymbol{r}\right)\sum_{\boldsymbol{G}} c_{\boldsymbol{G}}\mathrm{e}^{(\mathrm{i}(\boldsymbol{k}+\boldsymbol{G})\cdot\boldsymbol{r})} = \\ = E_{\boldsymbol{k}}\sum_{\boldsymbol{G}} c_{\boldsymbol{G}}\mathrm{e}^{(\mathrm{i}(\boldsymbol{k}+\boldsymbol{G})\cdot\boldsymbol{r})}\end{aligned} \tag{A.4}$$

Multiplication of the Eq.(A.4) by the orthogonal function $\exp\left(-\mathrm{i}\boldsymbol{G'}\cdot\boldsymbol{r}\right)$ and subsequent integration over the unit cell yields to the solution of the Schrödinger equation written in form

$$\frac{\hbar^2}{3m_e}\sum_{\boldsymbol{G}} c_{\boldsymbol{G}}\left|\boldsymbol{k}+\boldsymbol{G}\right|^2\delta\left(\boldsymbol{G}-\boldsymbol{G'}\right) + \sum_{\boldsymbol{G}} c_{\boldsymbol{G}}V\left(\boldsymbol{G}-\boldsymbol{G'}\right) = E_{\boldsymbol{k}}\sum_{\boldsymbol{G}} c_{\boldsymbol{G}}\delta\left(\boldsymbol{G}-\boldsymbol{G'}\right) \tag{A.5}$$

where

$$V\left(\boldsymbol{G}-\boldsymbol{G'}\right) = 1/\Omega\int V^{\text{pseudo}}\exp\left(\left(\boldsymbol{G}-\boldsymbol{G'}\right)\cdot\boldsymbol{r}\right) \tag{A.6}$$

represents a Fourier components of the pseudopotential V^{pseudo}. If there is only one atom in the primitive cell, the Fourier components are known as *pseudopotential form factors* V. In the case, when there are several atoms per primitive cell, it is convenient to define pseudopotential form factors and structure factors S depending strictly just on the position of particular atom in the primitive cell separately. For zinc–blende–type semiconductors which are represented by FCC primitive cell obtaining two different atoms (such as HgTe), the pseudopotential V^{pseudo} can be written as [97]

$$V^{\text{pseudo}} = \sum_{\boldsymbol{G'}}\left(S^s_{\boldsymbol{G'}}V^s_{\boldsymbol{G'}} + \mathrm{i}S^a_{\boldsymbol{G'}}V^a_{\boldsymbol{G'}}\right)\exp\mathrm{i}\left(\left(\boldsymbol{G}-\boldsymbol{G'}\right)\cdot\boldsymbol{r}\right), \tag{A.7}$$

where indices s and a mean symmetric and antisymmetric, respectively, and individual factors are given by

$$\begin{aligned} V^s_{\boldsymbol{G'}} &= \frac{1}{2}\left(V_1+V_2\right) \quad S^s_{\boldsymbol{G'}} = \cos\left(\boldsymbol{G'}\cdot\boldsymbol{r}\right) \\ V^a_{\boldsymbol{G'}} &= \frac{1}{2}\left(V_1-V_2\right) \quad S^a_{\boldsymbol{G'}} = \sin\left(\boldsymbol{G'}\cdot\boldsymbol{r}\right) \end{aligned} \tag{A.8}$$

The advantage of empirical pseudopotential method is that a small number of these factors are sufficient for calculating a bandstructure and they are commonly obtained from experiments.

Appendix B

Spatially Averaged Probability

In the supplementary materials of [72] it is formally demonstrated that, within an effective medium framework, the relation between the spatially averaged probability density associated with a Bloch energy eigenstate and the macroscopic wave function is such that:

$$\left\langle |\psi|^2 \right\rangle = \left(1 - \frac{\partial \hat{H}_{\text{eff}}}{\partial E}\right) |\psi_{\text{eff}}|^2 \tag{A1}$$

In the above, $\hat{H}_{\text{eff}}\left(E, \boldsymbol{k}\right)$ represents the homogenized (energy–dependent) Hamiltonian with $\boldsymbol{k} = -\mathrm{i}\nabla$. In this work, the effective medium Hamiltonian is given by [see Eq. (1.23)]:

$$\hat{H}_{\text{eff}}\left(E, \boldsymbol{k}\right) = \frac{\hbar^2 k^2}{2m} + V_{\text{eff}}. \tag{A2}$$

Hence, it follows that:

$$\left\langle |\psi|^2 \right\rangle = \left(1 - \frac{\partial V_{\text{eff}}}{\partial E}\right) |\psi_{\text{eff}}|^2 - \frac{\partial}{\partial E}\left(\frac{1}{m}\right) \frac{\hbar^2}{2} |i\mathbf{k}\psi_{\text{eff}}|^2. \tag{A3}$$

For a Bloch energy eigenstate in a continuous medium, we have $i\boldsymbol{k}\psi_{\text{c}} = \nabla\psi_{\text{c}}$, and thus the above result leads to Eq. (1.22) of the main text.

Bibliography

[1] J. Wen, Y. Zhang, and M. Xiao. The talbot effect: recent advances in classical optics, nonlinear optics, and quantum optics. *Adv. In Opt. and Photon*, 5:83, 2013.

[2] M. Berry, I. Marzoli, and W. Schleich. Quantum carpets, carpets of light. *Physics World*, June, 2001.

[3] J. D. Joannopoulos, S. G. Johnson, J. N. Winn, and R. D. Meade. *Photonic Crystals: Molding the Flow of Light.* Princeton University Press, 2nd edition, 2008.

[4] J. C. Knight. Photonic crystal fibres. *Nature*, 424:847, 2003.

[5] P. Russell. Photonic crystal fibers. *Science*, 299:358, 2003.

[6] A. Bjarklev, J. Broeng, and A. S. Bjarklev. *Photonic Crystal Fibres.* Springer Science & Business Media, 2012.

[7] A. Bruyant, G. Lérondel, P. J. Reece, and M. Gal. All-silicon omnidirectional mirrors based on one-dimensional photonic crystals. *Appl. Phys. Lett*, 82:3227, 2003.

[8] D. Labilloy, H. Benisty, C. Weisbuch, T.F. Krauss, V. Bardinal, and U. Oesterle. Demonstration of cavity mode between two-dimensional photonic-crystal mirrors. *Electronics Letters*, 33:1978, 1997.

[9] H.-J. Choi nad S. Choi, Y.-E. Yoo, E. ch. Jeon, Y. Yi, S. Park, D.-S. Choi, and H. Kim. Transmission-type photonic crystal structures for color filters. *Optics Express*, 21:18317, 2013.

[10] M. Bayindir, B. Temelkuran, and E. Ozbay. Photonic-crystal-based beam splitters. *Appl. Phys. Lett.*, 77:3902, 2000.

[11] T. Liu, A. R. Zakharian, M. Fallahi, J. V. Moloney, and M. Mansuripur. Multimode interference-based photonic crystal waveguide power splitter. *Journal of Lightwave Technology*, 22:2842, 2004.

[12] V. Agarwal, J. A. del Río, G. Malpuech, M. Zamfirescu, A Kavokin, D. Coquillat, D. Scalbert, M. Vladimirova, and B. Gil. Photon bloch oscillations in porous silicon optical superlattices. *Phys. Rev. Lett.*, 92:097401, 2004.

[13] F. Bloch. Über die quantenmechanik der elektronen in kristallgittern. *Zeit. Phys*, 52:555, 1929.

[14] C. Zener. A theory of the electrical breakdown of solid dielectrics. *Proc. R. Soc. London Ser. A*, 145:523, 1934.

[15] C. Waschke, H. Roskos, R. Schwedler, K. Leo, H. Kurz, and K. Köhler. Coherent submillimeter-wave emission from bloch oscillations in a semiconductor superlattice. *Phys. Rev. Lett.*, 70:3319, 1993.

[16] J. von Neumann and E. Wigner. Über merkwürdige diskrete eigenwerte. *Phys. Z.*, 30:465, 1929.

[17] F. H. Stillinger and D. R. Herrick. Coherent potential approximation: Basic concepts and applications. *Phys. Rev. A*, 11:446, 1975.

[18] E. N. Bulgakov, K. N. Pichugin, and I. Rotter. Bound states in the continuum in open Aharonov–Bohm ring. *JETP Letters*, 84:430–435, 2006.

[19] A F. Sadreev, E. N. Bulgakov, and I. Rotter. Bound states in the continuum in open quantum billiards with a variable shape. *Phys. Rev. B*, 73:23534, 2006.

[20] N. Moiseyev. Suppression of Feshbach resonance widths in two-dimensional waveguides and quantum dots: A lower bound for the number of bound states in the continuum. *Phys. Rev Lett.*, 102:167404, 2009.

[21] A. Albo, D. Fekete, and G. Bahir. Electronic bound states in the continuum above (Ga,In)(As,N)/(Al,Ga)As quantum wells. *Phys. Rev. B*, 85:115307, 2012.

[22] N. A. Gippius, S. G. Tikhodeev, and T. Ishihara. Optical properties of photonic crystal slabs with an asymmetrical unit cell. *Phys. Rev. B*, 72:045138, 2005.

[23] A. G. Borisov, F. J. García de Abajo, and S. V. Shabanov. Role of electromagnetic trapped modes in extraordinary transmission in nanostructured materials. *Phys. Rev. B*, 71:075408, 2005.

[24] D. C. Marinica, A. G. Borisov, and S. V. Snabanov. Bound states in the continuum in photonics. *Phys. Rev. Lett.*, 100:183902, 2008.

[25] M. G. Silveirinha. Trapping light in open plasmonic nanostructures. *Phys. Rev. A*, 89:023813, 2014.

[26] F. Monticone and A. Alu. Embedded photonic eigenvalues in 3d nanostructures. *Phys. Rev. Lett.*, 112:213903, 2014.

[27] Y. Plotnik, O. Peleg, F. Dreisow, M. Heinrich, S. Nolte, A. Szameit, and M. Segev. Experimental observation of optical bound states in the continuum. *Phys. Rev. Lett.*, 107:183901, 2011.

[28] J. Lee, B. Zhen, S.-L. Chua, W. Qiu, J. D. Joannopoulos, M. Soljacic, and O. Shapira. Observation and differentiation of unique high-Q optical resonances near zerowave vector in macroscopic photonic crystal slabs. *Phys. Rev. Lett.*, 109:067401, 2012.

[29] L. Golstone and A. A. Oliner. Leaky-wave antennas i: Rectangular waveguides. *Antennas and Propagation, IRE Transactions on*, 7:307, 1959.

[30] S. Monticone and A. Alu. Leaky-wave theory, techniques, and applications: From microwaves to visible frequencies. *Proc. IEEE*, 103:793, 2015.

[31] Ch. W. Hsu, B. Zhen, J. Lee, S.-L. Chua, S. G. Johnson, J. D. Joannopoulos, and M. Soljacic. Observation of trapped light within the radiation continuum. *Nature*, 499:188, 2013.

[32] D. Dragoman and M. Dragoman. The modeling of the quantum tunneling time through heterostructures using optical layered media. *Opt. Commun.*, 133:129, 1997.

[33] D. Dragoman and M. Dragoman. Optical modeling of quantum wire arrays. *IEEE J. Quantum Electron.*, 33:375, 1997.

[34] D. Dragoman and M. Dragoman. Optical modelling of quantum dots. *Opt. Commun.*, 150:331, 1997.

[35] J. Spector, H. L. Stormer, K. W. Baldwin, L. N. Pfeiffer, and K. W. West. Electron focusing in two-dimensional systems by means of an electrostatic lens. *Appl. Phys. Lett.*, 56:1290, 1990.

[36] J. H. Smet, D. Weiss, R. H. Blick, G. Lütjering, and K. von Klitzing. Magnetic focusing of composite fermions through arrays of cavities. *Phys. Rev. Lett.*, 77:2272, 1996.

[37] U. Sivan, M. Heiblum, C. P. Umbach, and H. Shtrikman. Electrostatic electron lens in the ballistic regime. *Phys. Rev. E*, 41:7937, 1990.

[38] J. Spector, H. L. Stormer, K. W. Baldwin, L. N. Pfeiffer, and K. W. West. Refractive switch for two-dimensional electrons. *Appl. Phys. Lett.*, 56:2433, 1990.

[39] R. C. Liu, B. Odom, Y. Yamamoto, and S. Tarucha. Quantum interference in electron collision. *Nature*, 391:263, 1998.

[40] J. A. del Alamo and C. C. Euster. Quantum field-effect directional coupler. *Appl. Phys. Lett.*, 56:78, 1989.

[41] M. Thomas, N. Dagli, J. Waldman, and A. Gossard. Zero gap electron waveguide coupler. *Integrated Photon. Res. Proc.*, 10:103, 1993.

[42] T. K. Gaylord, E. N. Glytsis, and K. F. Brennan. Semiconductor superlattice interference filter design. *J. Appl. Phys.*, 65:2535, 1989.

[43] A. N. Khondker, M. Rezwan Khan, and A. F. M. Anwar. Transmission line analogy of resonance tunneling phenomena: The generalized impedance concept. *J. Appl. Phys.*, 63:5191, 1988.

[44] R. Marqués, F. Martín, and M. Sorolla. *Metamaterials with Negative Parameters: Theory and Microwave Applications*. John Wiley & Sons, Inc., 2007.

[45] L. Solymar and E. Shamonina. *Waves in Metamaterials*. Oxford University Press, 2009.

[46] J. B. Pendry. Negative refraction makes a perfect lens. *Phys. Rev. Lett.*, 85:3966, 2000.

[47] U. Leonhardt. Optical conformal mapping. *Science*, 312:1777, 2006.

[48] J. B. Pendry, D. Schurig, and D. R. Smith. Controlling electromagnetic fields. *Science*, 312:1780, 2006.

[49] K. Kobayashi. Complementary media of electrons. *J. Phys.–Condens. Mat.*, 18:3703, 2006.

[50] D. Dragoman and M. Dragoman. Metamaterials for ballistic electrons. *J. Appl. Phys.*, 101:104316, 2007.

[51] V. V. Cheianov, V. Falko, and B. L. Altshuler. The focusing of electron flow and a veselago lens in graphene p-n junctions. *Science*, 315:1252, 2007.

[52] S. Zhang, D. A. Genov, C. Sun, and X. Zhang. Cloaking of matter waves. *Phys. Rev. Lett.*, 100:(2008), 2008.

[53] L. Jelinek, J. D. Baena, J. Voves, and R. Marques. Metamaterial-inspired perfect tunnelling in semiconductor heterostructures. *New J. Phys.*, 13:083011, 2011.

[54] M. G. Silveirinha and N. Engheta. Effective medium approach to electron waves: Graphene superlattices. *Phys. Rev. B*, 85:195413, 2012.

[55] M. G. Silveirinha and N. Engheta. Metamaterial-inspired model for electron waves in bulk semiconductors. *Phys. Rev. B*, 86:245302, 2012.

[56] R. Fleury and A. Alu. Exotic properties and potential applications of quantum metamaterials. *Appl. Phys. A*, 109:781, 2012.

[57] M. G. Silveirinha and N. Engheta. Transformation electronics: Tailoring the effective mass of electrons. *Phys. Rev. B*, 86:161104, 2012.

[58] R. Fleury and A. Alu. Quantum cloaking based on scattering cancellation. *Phys. Rev. B*, 87:045423, 2013.

[59] K. Gottfried and T.-M. Yan. *Quantum mechanics: Fundamentals*, page 620. Springer, 2nd edition, 2003.

[60] N. W. Aschroft and N. D. Mermin. *Solid State Physics*. Holt, Rinehart and Winston, 1976.

[61] P. Hohenberg and W. Kohn. Inhomogeneous electron gas. *Phys. Rev.*, 136:B864–B871, Nov 1964.

[62] J. C. Slater and G. F. Koster. Simplified lcao method for the periodic potential problem. *Phys. Rev.*, 94:1498–1524, Jun 1954.

[63] D. J. Chadi and M. L. Cohen. Tight-binding calculations of the valence bands of diamond and zincblende crystals. *physica status solidi (b)*, 68(1):405–419, 1975.

[64] James R. Chelikowsky and Marvin L. Cohen. Nonlocal pseudopotential calculations for the electronic structure of eleven diamond and zinc-blende semiconductors. *Phys. Rev. B*, 14:556–582, Jul 1976.

[65] E. O. Kane. Band structure of indium antimonide. *J. Phys. Chem. Sol.*, 1:249, 1957.

[66] G. Bastard. Superlattice band structure in the envelope-function approximation. *Phys. Rev. B*, 24:5693, 1981.

[67] S. Flugge. *Practical Quantum Mechanics - Volume 1 and Volume 2*. Springer, 1971.

[68] G. Bastard. *Wave Mechanics Applied to Semiconductor Heterostructures*. John Wiley & Sons, 1988.

[69] G. Bastard and J. A. Brum. Electronic states in semiconductor heterostructures. *IEEE J. Quantum Elect.*, 22:1625, 1986.

[70] S. Lannebère and M. G. Silveirinha. Effective Hamiltonian for electron waves in artificial graphene: A first-principles derivation. *Phys. Rev. B*, 91:045416, 2015.

[71] G. Bastard. Theoretical investigations of superlattice band structure in the envelope-function approximation. *Phys. Rev. B*, 25:7584, 1982.

[72] D. E. Fernandes, N. Engheta, and M. G. Silveirinha. Wormhole for electron waves in graphene. *Phys. Rev. B*, 90:041406(R), 2014.

[73] F. N. H. Robinson. *Macroscopic electromagnetism*. Pergamon Press, 1 edition, 1973.

[74] L. Suttorp S. deGroot. *Foundations of Electrodynamcs*, page 535. North–Holland, 1972.

[75] R. F. Harrington. *Time-Harmonic Electromagnetic Fields*. New York: John Wiley and Sons, Inc., 2001.

[76] S. Bloom and T. K. Bergstresser. Band structure of hgse and hgte. *Phys. Stat. Sol*, 42:191, 1970.

[77] W. Potz and P. Vogl. Theory of optical-phonon deformation potentials in tetrahedral semiconductors. *Phys. Rev. B*, 24:2025, 1981.

[78] S. Mecabih, N. Amrane, B. Belgoumene, and H. Aourag. Opto-electronic properties of the ternary alloy hg1-xcdxte. *Physica A*, 276:495, 2000.

[79] S. F. Mahmound. *Electromagnetic Waveguides: Theory and Applications*. Peregrinus Ltd., 1991.

[80] D. M. Pozar. *Microwave Engeneering*, page 700. John Wiley and Sons, Inc., 3rd edition, 2001.

[81] W. Greiner and D. A. Bromley. *Quantum mechanics: An Indroduction*, page 489. Berlin: Springer, 4th edition, 2001.

[82] H. Feshbach. Unified theory of nuclear reactions. *Annals of Physics (N.Y.)*, 5:357, 1958.

[83] R. G. Newton. *Scattering Theory of Waves and Particles*. Springer-Verlag, 2nd edition, 2013.

[84] F. Capasso, C. Sirtori, J. Faist, D. L. Sivco, S.-N. G. Chu, and A. Y. Cho. Observation of an electronic bound states above a potential well. *Nature*, 358:565, 1992.

[85] T. A. Weber. Bound states with no classical turning points in semiconductor heterostructures. *Solid State Commun.*, 90:713, 1994.

[86] G.B. Arfken and H.J. Weber. *Mathematical Methods for Physicists*, page 981. Harcourt/Academic Press, 5th edition, 2001.

[87] C. A. Balanis. *Advanced Engineering Electromagnetics*. John Wiley & Sons, 2nd edition, 2012.

[88] T. K. Gaylord, G. N. Henderson, and E. N. Glytsis. Application of electromagnetics formalism to quantum-mechanical electron-wave propagation in semiconductors. *J. Opt. Soc. Am. B*, 10:333, 1993.

[89] D. Dragoman and M. Dragoman. Optical analogue structures to mesoscopic devices. *Prog. Quant. Electron.*, 23:131, 1999.

[90] G. L. Hansen, J. L. Schmitt, and T. N. Casselman. Energy gap versus alloy composition and temperature in $Hg_{1--x}Cd_xTe$. *J. Appl. Phys.*, 53:7099, 1982.

[91] A. Rogalski. Hgcdte infrared detector material: history, status and outlook. *Rep. Prog. Phys.*, 68:2267, 2005.

[92] S. P. Kowalczyk, J. T. Cheung, E. A. Kraut, and R. W. Grant. CdTe-HgTe (111) heterojunction valence-band discontinuity: A common-anion-rule contradiction. *Phys. Rev. Lett.*, 56:1605, 1986.

[93] John D. Wiley and R. N. Dexter. Helicons and nonresonant cyclotron absorption in semiconductors. ii. $Hg_{1-x}Cd_xTe$. *Phys. Rev.*, 181:1181–1190, May 1969.

[94] M. G. Silveirinha and N. Engheta. Giant nonlinearity in zero-gap semiconductor superlattices. *Phys. Rev. B*, 89:085205, 2014.

[95] J. D. Jackson. *Classical Electrodynamics*. John Wiley & Sons, Inc., 3rd edition, 1998.

[96] P. M. Morse and H. Feshbach. *Methods of Theoretical Physics*. McGraw-Hill Book Company, Inc., 1953.

[97] J. C. Phillips. Energy-band interpolation scheme based on a pseudopotential. *Phys. Rev.*, 112:685, 1958.

[98] J.C. Phillips and L. Kleinman. New method for calculating wave functions in crystals and molecules. *Phys. Rev.*, 116:287, 1959.

[99] L. Kleinman and J.C. Phillips. Crystal potential and energy bands of semiconductors. iii. self-consistent calculations for silicon. *Phys. Rev.*, 118:1153, 1960.

Publications

List of author's publications related to the doctoral thesis

All authors contributed equally unless otherwise stated.

Papers in Peer–Reviewed Journals with Impact Factor

[A1] I. Hrebikova, L. Jelinek, M. G. Silveirinha, "Embedded energy state in an open semiconductor heterostructure," *Phys. Rev. B*, vol. 92, p. 155303, 2015, doi: 10.1103/PhysRevB.92.155303.

[A2] I. Hrebikova, L. Jelinek, J. Voves, J. D. Beana, "A perfect lens for ballistic electrons: An electron–light wave analogy," *Photonics Nanostructures: Fundam. Appl.*, vol. 12, p. 9-15, 2014, doi: 10.1016/j.photonics.2013.08.005.

Papers and Abstracts in Conference Proceedings Listed in the Web of Knowledge

[B1] I. Hrebikova, L. Jelinek, M. G. Silveirinha, "Bound states within the continuum – A metamaterial–semiconductor analogy," *9TH INTERNATIONAL CONGRESS ON ADVANCED ELECTROMAGNETIC MATERIALS IN MICROWAVES AND OPTICS (METAMATERIALS 2015)*,Oxford, England, 07-12 September, 2015.

[B2] I. Hrebikova, L. Jelinek, J. Voves, J. D. Beana, "A perfect lens for ballistic electrons," *7th International Congress on Advanced Electromagnetic Materials in Microwaves and Optics - Metamaterials 2013*, Bordeaux, France, 16-21 September 2013.

Citations in Web of Knowledge and SCOPUS

[A1] cited at E. N. Bulgakov, A. F. Saadrev,"Spin polarized bound states in the continuum in open Aharonov-Bohm rings with the Rashba spin-orbit interaction",*JOURNAL OF PHYSICS-CONDENSED MATTER*, vol. 28, iss. 26, 2016

[A1] cited at Ch. W. Hsu, B. Zhen, A. D. Stone, et.al., "Bound states in the continuum", *NATURE REVIEWS MATERIALS*, vol. 1, iss. 9, 2016

[A1] cited at E. N. Bulgakov, A. F. Saadrev, "Transfer of spin angular momentum of an incident wave into orbital angular momentum of the bound states in the continuum in an array of dielectric spheres", *PHYSICAL REVIEW A*, vol. 94, iss. 3, 2016

[A1] cited at E. N. Bulgakov, A. F. Saadrev,D. N. Maksimov, "Light Trapping above the Light Cone in One-Dimensional Arrays of Dielectric Spheres", *APPLIED SCIENCES-BASEL*,vol. 7, iss. 2, 217

[A1] cited at A. S. Pilipchuck, A.F. Saadrev,"Accidental bound states in the continuum in an open Sinai billiard", *PHYSICS LETTERS A*, vol. 381, iss. 7, 2017

[A1] cited at A. F. Saadrev, A. S. Pilipchuck, A. A. Lyapina, "Tuning of Fano resonances by rotation of continuum: Wave faucet", *EPL*, vol. 117, iss. 5, 2017

[A1] cited at S. Solange, T. A. Morgado, M. G. Silveirinha, "Discrete Light Spectrum of Complex–Shaped Meta–atoms", *RADIO SCIENCE*, vol. 53, iss. 2, 2018

[A2] cited at M. G. Silveirinha, N. Engheta, "Giant nonlinearity in zero–gap semiconductor superlattices", *PHYSICAL REVIEW B*, vol. 89, iss. 8, 2014

[A2] cited at D. E. Fernandes, N. Engheta, M. G. Silveirinha, "Wormhole for electron waves in graphene", *PHYSICAL REVIEW B*, vol. 90, iss. 4, 2014

[A2] cited at R. Fleury, A. Alu, " Manipulation of electron flow using near-zero index semiconductor metamaterials", *PHYSICAL REVIEW B*, vol. 90, iss. 3, 2014

[A2] cited at M. R. C. Mahdy, A. Al Sayem, A. Shahriar, et al., "Electromagnetic metamaterial-inspired band gap and perfect transmission in semiconductor and graphene-based electronic and photonic structures", *EUROPEAN PHYSICAL JOURNAL PLUS* , vol. 131, iss. 4, 2016

[A2] cited at J. H. Vargas, R. E. Castublanco, J. Morales, "LIGHT-ELECTRON WAVE ANALOGY APPLIED TO THE OPTICAL SYSTEM DIELECTRIC-SUBSTRATE FOR PHYSICS COURSES", *MOMENTO-REVISTA DE FISICA*, iss. 54, 2017

[A2] cited at W. Huang, S. Liang, E. Kzoseva, et al., "A Novel Design of Ultrafast Electron Switching Device", *Conference on Lasers and Electro-Optics Pacific Rim (CLEO-PR)*, Singapore, SINGAPORE, JUL 31-AUG 04, 2017

[A2] cited at W. Huang, S. Liang, E. Kzoseva, et al., "A new coupling mechanism between two graphene electron waveguides for ultrafast switching", *SEMICONDUCTOR SCIENCE AND TECHNOLOGY*, vol. 33, iss. 3, 2018

List of author's publications non–related to the doctoral thesis

All authors contributed equally unless otherwise stated.

Papers in Peer–Reviewed Journals with Impact Factor

[C1] M. Koys, I. Bugar, I. Hrebikova, et al., "Spectral switching control of ultrafast pulses in dual core photonic crystal fibre",*JOURNAL OF THE EUROPEAN OPTICAL SOCIETY*,vol. 8, 2013

Papers and Abstracts in Conference Proceedings Listed in the Web of Knowledge or SCOPUS

[D1] I. Hrebikova, M. Grajcar, P. Neilinger, et al., "Tunable superconducting metamaterials," *17th Conference of Czech and Slovak Physicists*, Zilina, Slovakia, 5-8 September 2011.

Citations in Web of Knowledge and SCOPUS

[C1] cited at P. Stajanca, R. Buczynski, G. Andriukaitis, et al., "Ultrafast Solitonic Nonlinear Directional Couplers Utilizing Multicomponent Glass Dual-Core Photonic Crystal Fibres", *16th International Conference on Transparent Optical Networks (ICTON)*, Graz, Austria, 6-10 July, 2014

[C1] cited at P. Stajanca, D. Pysz, M. Michalka, et al., " Soliton-based ultrafast multi-wavelength nonlinear switching in dual-core photonic crystal fibre", *LASER PHYSICS*, vol. 24, iss. 6, 2014

[C1] cited at P. Stajanca, D. Pysz, G. Andriukaitis, et al., " Ultrafast multi-wavelength switch based on spectrally–shifted solitons dynamics in a dual-core photonic crystal fiber", *OPTIC EXPRESS*, vol. 22, iss. 25, 2014

[C1] cited at P. Stajanca, I. Bugar, "Nonlinear ultrafast switching based on soliton self-trapping in dual-core photonic crystal fibre", *LASER PHYSICS LETTERS*, vol. 13, iss. 11, 2016

[C1] cited at L. Currila, I. Astrauskas, A. Pugzlys, et al., "Towards ultrafast sub-nanojoule solitonic nonlinear directional coupler based on soft glass dual–core photonics crystal fibers", *Conference on Micro-Structured and Specialty Optical Fibres V* , Strabourg, France, 25-26 April, 2018

[C1] cited at L. Currila, I. Astrauskas, A. Pugzlys, et al., "Nonlinear performance of asymmetric coupler based on dual-core photonic crystal fiber: Towards sub-nanojoule solitonic ultrafast all-optical switching", *OPTICAL FIBER TECHNOLOGY*, vol. 42, p. 39-49, 2018